Available online at www.sciencedirect.com

ScienceDirect

Remote Sensing of Environment 111 (2007) 519–536

Remote Sensing of Environment

www.elsevier.com/locate/rse

Development of a global evapotranspiration algorithm based on MODIS and global meteorology data

Qiaozhen Mu *, Faith Ann Heinsch, Maosheng Zhao, Steven W. Running

Numerical Terradynamic Simulation Group (NTSG), College of Forestry & Conservation, The University of Montana, 32 Campus Drive, Missoula, MT 59812, USA

Received 9 August 2006; received in revised form 10 April 2007; accepted 14 April 2007

Abstract

The objective of this research is to develop a global remote sensing evapotranspiration (ET) algorithm based on Cleugh et al.'s [Cleugh, H.A., R. Leuning, Q. Mu, S.W. Running (2007) Regional evaporation estimates from flux tower and MODIS satellite data. *Remote Sensing of Environment* 106, page 285–304- 2007 (doi: 10.1016/j.rse.2006.07.007).] Penman–Monteith based ET (RS-PM). Our algorithm considers both the surface energy partitioning process and environmental constraints on ET. We use ground-based meteorological observations and remote sensing data from the MODerate Resolution Imaging Spectroradiometer (MODIS) to estimate global ET by (1) adding vapor pressure deficit and minimum air temperature constraints on stomatal conductance; (2) using leaf area index as a scalar for estimating canopy conductance; (3) replacing the Normalized Difference Vegetation Index with the Enhanced Vegetation Index thereby also changing the equation for calculation of the vegetation cover fraction (F_C); and (4) adding a calculation of soil evaporation to the previously proposed RS-PM method.

We evaluate our algorithm using ET observations at 19 AmeriFlux eddy covariance flux towers. We calculated ET with both our Revised RS-PM algorithm and the RS-PM algorithm using Global Modeling and Assimilation Office (GMAO v. 4.0.0) meteorological data and compared the resulting ET estimates with observations. Results indicate that our Revised RS-PM algorithm substantially reduces the root mean square error (RMSE) of the 8-day latent heat flux (LE) averaged over the 19 towers from 64.6 W/m^2 (RS-PM algorithm) to 27.3 W/m^2 (Revised RS-PM) with tower meteorological data, and from 71.9 W/m^2 to 29.5 W/m^2 with GMAO meteorological data. The average LE bias of the tower-driven LE estimates to the LE observations changed from 39.9 W/m^2 to −5.8 W/m^2 and from 48.2 W/m^2 to −1.3 W/m^2 driven by GMAO data. The correlation coefficients increased slightly from 0.70 to 0.76 with the use of tower meteorological data. We then apply our Revised RS-PM algorithm to the globe using 0.05° MODIS remote sensing data and reanalysis meteorological data to obtain the annual global ET (MODIS ET) for 2001. As expected, the spatial pattern of the MODIS ET agrees well with that of the MODIS global terrestrial gross and net primary production (MOD17 GPP/NPP), with the highest ET over tropical forests and the lowest ET values in dry areas with short growing seasons. This MODIS ET product provides critical information on the regional and global water cycle and resulting environment changes.

Keywords: Evapotranspiration; Stomatal conductance; Soil evaporation; Vegetation cover fraction; Remote sensing; Meteorological data; MODIS

1. Introduction

Evapotranspiration (ET), the sum of water lost to the atmosphere from the soil surface through evaporation and from plant tissues via transpiration, is a vital component of the water cycle, which includes precipitation, runoff, streamflow, soil water storage and ET. High correlation was observed between stomatal conductance and the rate of carbon assimilation for a wide range of plant species (Korner, 1994; McMurtrie et al., 1992). Stomatal conductance controls the rate of water and carbon exchange between vegetation and the atmosphere (Cowan, 1977; Cowan & Farquhar, 1977; Farquhar et al., 2002; Hari et al., 1986). In general, high stomatal conductance leads to high transpiration and high photosynthesis, resulting in lowering of soil moisture assuming there are no additional inputs of water, which in turn reduces the stomatal conductance (Dang et al., 1997; Jarvis, 1976; Kawamitsu et al., 1993; Marsden et al., 1996; Misson et al., 2004; Oren et al., 1999; Sandford & Jarvis, 1986). Over a relatively long time period (i.e., a season or a year), the water available for humans and ecosystems in a given region can be approximated by the difference between accumulated precipitation and ET

* Corresponding author. Tel.: +1 406 243 6218; fax: +1 406 243 4510.
E-mail address: qiaozhen@ntsg.umt.edu (Q. Mu).

0034-4257/$ - see front matter © 2007 Elsevier Inc. All rights reserved.
doi:10.1016/j.rse.2007.04.015

(Donohue et al., 2007). With an increasing human population and rapid climate change, water has become a great concern both for the environment and society. Accurate knowledge of temporal and spatial variations in precipitation and ET is critical for improved understanding of the interactions between land surfaces and the atmosphere, and it is crucial for improving water and land resource management (Dodds et al., 2005; Meyer, 1999; Raupach, 2001), drought detection and assessment (McVicar & Jupp, 1998), and regional hydrological applications (Keane et al., 2002; Kustas & Norman, 1996; Rango & Shalaby, 1998). However, precipitation and ET are the most problematic components of the water cycle to estimate accurately because of the heterogeneity of the landscape and the large number of controlling factors involved, including climate, plant biophysics, soil properties, and topography (Friedl, 1996; Gash, 1987; Janowiak et al., 1998; Maddock et al., 1998; Vörösmarty et al., 1998; http://dx.doi.org/10.1016/j.jhydrol.2007.02.018). Remotely sensed data, especially those from polar-orbiting satellites, provide us with temporally and spatially continuous information over vegetated surfaces and are useful for accurately parameterizing surface biophysical variables, such as albedo, biome type and leaf area index (LAI) (Los et al., 2000). The MODerate Resolution Imaging Spectroradiometer (MODIS) onboard NASA's Terra and Aqua satellites, provide unprecedented information regarding vegetation and surface energy (Justice et al., 2002), which can be used to develop a remotely sensed ET model.

Calculation of ET is typically based on the conservation of either energy or mass, or both. Computing ET is a combination of two complicated major issues: (1) estimating the stomatal conductance to derive transpiration from plant surfaces; and (2) estimating evaporation from the ground surface. Plant transpiration is controlled by canopy conductance, which further represents the average status of leaf level stomatal conductance. Stomatal conductance is sensitive to diurnal changes in absorbed photosynthetically active radiation (APAR = FPAR * IPAR, IPAR = 0.45 * Rsw, Rsw: the incident shortwave radiation; IPAR: the photosynthetically active radiation incident on the vegetative surface; FPAR: the fraction of IPAR absorbed by the vegetative surface), vapor pressure deficit, leaf temperature, hydraulic conductance within the plant, and soil moisture near the roots (Dang et al., 1997; Jarvis, 1976; Kawamitsu et al., 1993; Marsden et al., 1996; Misson et al., 2004; Oren et al., 1999; Sandford & Jarvis, 1986). Therefore, a fluctuation in stomatal conductance usually leads to a commensurately large fluctuation in transpiration, and hence, ET. In semiarid or arid systems, soil evaporation is a major component of ET, yet little is known quantitatively about it over large spatial scales. Soil evaporation is reported to range from a few percent to more than 80% of the measured or estimated total ET depending on the vegetation cover (Bethenod et al., 2000; Hsiao & Xu, 2005; Villalobos & Fereres, 1990; Wilson et al., 2000).

As a result, developing a robust algorithm to estimate global evapotranspiration is a significant challenge. Traditional energy balance models of ET require explicit characterization of numerous physical parameters, many of which are difficult to determine globally. For example, SEBAL (Bastiaanssen et al., 1998a,b), SEBS (Su, 2002), and RSEB (Kalma & Jupp, 1990) estimate ET as a residual of the energy balance at the earth's surface, which contain biases from both the sensible heat flux and net radiation. The REBM model (McVicar & Jupp, 1999, 2002) uses combined remote sensing data and meteorological data to calculate ET, while the triangle method (Gillies & Carlson, 1995; Nemani & Running, 1989; Nishida & Nemani, 2003) uses the slope of surface temperature versus the Normalized Difference Vegetation Index (NDVI) to estimate the surface resistance to ET, and the dual-source model developed by Norman et al. (1995) and Kustas and Norman (1999) uses multi-angular remote sensing. For these models, thermal remote sensing data (e.g., land surface temperature [LST]) are the most important inputs.

However, using the 8-day composite MODIS LST (the average LST of all cloud-free data in the compositing window) (Wan et al., 2002) and daily meteorological data recorded at the flux tower, Cleugh et al. (2007) demonstrate that the results from thermal models are unreliable at two Australian sites (Virginia Park, a wet/dry tropical savanna located in northern Queensland and Tumbarumba, a cool temperate, broadleaved forest in south east New South Wales). Using a combination of remote sensing and global meteorological data, we have adapted the Cleugh et al. (2007) algorithm, which is based on the Penman–Monteith method and calculates both canopy conductance and ET. In this paper, we describe the methodology used to develop the ET algorithm, verify the algorithm at 19 AmeriFlux towers in 2001, and apply the algorithm globally.

2. ET algorithm logic

Our ET algorithm is a revision to the algorithm proposed by Cleugh et al. (2007) (hereafter called RS-PM). Their algorithm is based on the Penman–Monteith (P–M) equation (Monteith, 1964):

$$\lambda E = \frac{sA + \rho C_p (e_{sat} - e)/r_a}{s + \gamma(1 + r_s/r_a)} \tag{1}$$

where λE (unit: W/m^2) is the latent heat flux and λ (J/kg) is the latent heat of evaporation; $s = d(e_{sat})/dT$ (unit: Pa/K) and is the slope of the curve relating saturated water vapor pressure (e_{sat}: Pa) to temperature; A (W/m^2) is available energy; ρ (kg/m^3) is air density; C_p (J/kg/K) is the specific heat capacity of air; e (Pa) is the actual water vapor pressure; and r_a (s/m) is the aerodynamic resistance. The psychrometric constant γ(Pa/K) is given by $\gamma = (M_a/M_w)(C_p P/\lambda)$, where M_a (kg/mol) and M_w (kg/mol) are the molecular masses of dry air and wet air, respectively, and P (Pa) is atmospheric pressure (Maidment, 1993). Surface resistance (r_s: s/m) is an effective resistance to evaporation from the soil surface and transpiration from the plant canopy. Input data to the algorithm include daily meteorology (temperature, actual vapor pressure, and incoming solar radiation) and remotely sensed LAI and NDVI. In addition, this algorithm is computed daily to take advantage of widely available daily meteorology, overcoming the obstacle of using the 8-day MODIS LST data. Cleugh et al. (2007) verified the RS-PM algorithm at the same two flux towers in

Australia with good agreement (root mean square error [RMSE]= 27 W/m^2, R^2=0.74). The RMSE is expressed as

$$\mathrm{RMSE} = \sqrt{\frac{\sum_{i=1}^{N} (\mathrm{LE}_{\mathrm{est}} - \mathrm{LE}_{\mathrm{obs}})^2}{N}} \quad (2)$$

where $\mathrm{LE}_{\mathrm{est}}$ is the estimated latent heat flux (LE) by the algorithm, $\mathrm{LE}_{\mathrm{obs}}$ represents the observed latent heat flux, and N is the total number of samples. The smaller the RMSE, the better able the model to estimate ET.

In RS-PM, the surface conductance is estimated by using NDVI and LAI, such that:

$$F_{\mathrm{C}} = \left(\frac{\mathrm{NDVI} - \mathrm{NDVI}_{\min}}{\mathrm{NDVI}_{\max} - \mathrm{NDVI}_{\min}}\right)^2$$

$$g_{\mathrm{s}} = c_{\mathrm{L}} \max(\mathrm{LAI}_{\min}, (F_{\mathrm{C}}\mathrm{LAI}_{\max})) \quad (3)$$

In Eq. (3), g_s (m/s) is the surface conductance and r_s (s/m) is the inverse of g_s; c_L (m/s) is the mean surface conductance per unit leaf area index; F_C is the fractional vegetation cover; and $\mathrm{NDVI}_{\min}$ and $\mathrm{NDVI}_{\max}$ are the minimum and maximum NDVI during the study period.

There are two major problems with Cleugh et al.'s (2007) RS-PM algorithm. First, they have used NDVI and LAI to calculate r_s, assuming that surface resistance is equal to canopy resistance and that soil evaporation is small enough to be neglected in comparison to transpiration from plants. Studies have demonstrated, however, that high ratios of soil evaporation to ET are often observed when the canopy cover (or LAI) is low and the soil surface is moist to wet most of the time (Hsiao & Xu, 2005). For example, Villalobos and Fereres (1990) measured soil evaporation to be 60%–80% of ET for sunflower, maize, and cotton with LAI of 0.6 to 1.2. As the crop canopy increases, covering a larger portion of the ground, soil evaporation decreases. Bethenod et al. (2000) studied maize with complete canopy cover (LAI$\approx$4.0) and found that soil evaporation was approximately 10% of total ET. Wilson et al. (2000) measured the energy balance above and below the canopy of a temperate deciduous forest ecosystem and found that, on an annual basis, the ET fluxes from the forest floor were 15%–22% of those above the canopy and the evaporation was 86 mm, or about 10% of the total ecosystem ET.

Second, there is no water stress or temperature constraint on canopy conductance in the RS-PM algorithm, which can result in large biases in dry or cold seasons. Saugier et al. (1997) measured the transpiration of a boreal pine forest in the southern Canada BOREAS study area. They observed that transpiration rates were low even when the soil was well supplied with water, attributing the low rates of transpiration to the canopy's low LAI and a marked reduction in stomatal conductance as vapor pressure deficits increased. To resolve these two issues, we have improved RS-PM algorithm as described in Sections 2.1 through 2.3 by (1) adding vapor pressure deficit and minimum air temperature constraints on stomatal conductance; (2) using leaf area index as a scalar for estimating canopy conductance; (3) replacing the Normalized Difference Vegetation Index with the Enhanced Vegetation Index, thereby also changing the equation for calculation of the vegetation cover fraction (F_C); and (4) adding a calculation of soil evaporation. Fig. 1 shows the logic behind the MODIS ET Algorithm for calculating daily MODIS ET.

2.1. Improvements to canopy conductance calculation

For many plant species, stomatal conductance (Cs) decreases as vapor pressure deficit (VPD) increases, and stomatal conductance is further limited by both low and high temperatures (Dang et al., 1997; Jarvis, 1976; Kawamitsu et al., 1993; Leuning, 1995; Marsden et al., 1996; Misson et al., 2004; Oren et al., 1999, 2001; Sandford & Jarvis, 1986; Schulze et al., 1994; Xu & Baldocchi, 2002). VPD is calculated as the difference between saturated air vapor pressure, as determined from air temperature (Murray, 1967), and actual air vapor pressure. Because high temperatures are often accompanied by high VPDs, we have only added constraints on stomatal conductance for VPD and minimum air temperature, ignoring constraints resulting from high temperature. We used LAI as a scalar to convert the stomatal conductance (Cs) calculated at the leaf level to a canopy conductance (Cc) (Landsberg & Gower, 1997):

$$C_{\mathrm{S}} = c_{\mathrm{L}} \times m(T\mathrm{min}) \times m(\mathrm{VPD})$$

$$Cc = Cs \times \mathrm{LAI} \quad (4)$$

where c_L is the mean potential stomatal conductance per unit leaf area, $m(T\mathrm{min})$ is a multiplier that limits potential stomatal conductance by minimum air temperatures (Tmin), and m(VPD) is a multiplier used to reduce the potential stomatal conductance when VPD is high enough to inhibit photosynthesis (Dang et al., 1997; Jarvis, 1976; Kawamitsu et al., 1993; Leuning, 1995; Marsden et al., 1996; Misson et al., 2004; Oren et al., 1999, 2001; Sandford & Jarvis, 1986; Schulze et al., 1994; Xu & Baldocchi, 2002). In the case of plant transpiration, surface conductance (g_s in Eq. (3)) is equal to the canopy conductance, and hence surface resistance (r_s) is the inverse of canopy conductance (Cc). The LAI in Eq. (4) is obtained from the global 8-day standard MODIS LAI product, which is estimated using a canopy radiation transfer model combined with remotely sensed surface reflectance data (Myneni et al., 2002). We calculate the constraints for minimum air temperature (Tmin) and VPD as:

$$m(T\mathrm{min}) = \begin{cases} 1.0 & T\mathrm{min} \geq T\mathrm{min\_open} \\ \dfrac{T\mathrm{min} - T\mathrm{min\_close}}{T\mathrm{min\_open} - T\mathrm{min\_close}} & T\mathrm{min\_close} < T\mathrm{min} < T\mathrm{min\_open} \\ 0.1 & T\mathrm{min} \leq T\mathrm{min\_close} \end{cases}$$

$$m(\mathrm{VPD}) = \begin{cases} 1.0 & \mathrm{VPD} \leq \mathrm{VPD\_open} \\ \dfrac{\mathrm{VPD\_close} - \mathrm{VPD}}{\mathrm{VPD\_close} - \mathrm{VPD\_open}} & \mathrm{VPD\_open} < \mathrm{VPD} < \mathrm{VPD\_open} \\ 0.1 & \mathrm{VPD} \geq \mathrm{VPD\_close} \end{cases} \quad (5)$$

where close indicates nearly complete inhibition (full stomatal closure) and open indicates no inhibition to transpiration (Table 1).

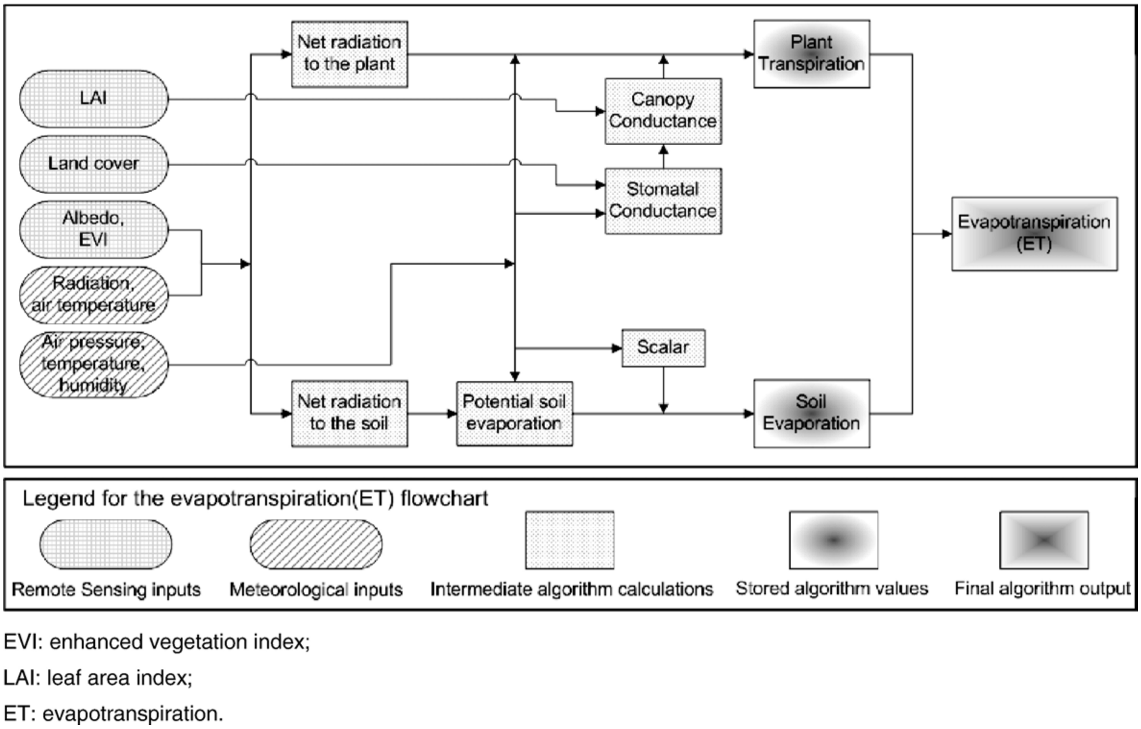

Fig. 1. Flowchart showing the logic behind the MODIS ET Algorithm for calculating daily MODIS ET.

When *T*min is lower than the threshold value *T*min_close, or VPD is higher than the threshold VPD_close, the temperature or the water stress will cause stomata to close almost completely, halting plant transpiration. On the other hand, when *T*min is higher than *T*min_open, and VPD is lower than VPD_open, there will be no temperature or water stress on transpiration. The multipliers range linearly from 0.1 (nearly total inhibition, limiting r_s) to 1 (no inhibition) for the range of biomes also used in the MOD17 GPP/NPP algorithm, which are listed in a Biome Properties Look-Up Table (BPLUT) (Table 1) (Heinsch et al., 2003; Running et al., 2004). Complete details on the derivation of the algorithm and the values used in the BPLUT can be found elsewhere (Heinsch et al., 2003; Running et al., 2000). The effect of soil water availability is not included in the ET algorithm. Some studies have suggested that atmospheric conditions reflect surface parameters (Bouchet, 1963; Morton, 1983), and VPD can be used as an indicator of environment water stress (Granger & Gray, 1989; Running & Nemani, 1988). In addition, Mu et al. (2007) found that VPD alone can capture interannual variability of the full water stress from both the atmosphere and soil for almost all of China and the conterminous U.S., though it may fail to capture the full seasonal water stress in dry regions experiencing strong summer monsoons.

2.2. Improvements on vegetation cover fraction

The Normalized Difference Vegetation Index (NDVI) and Enhanced Vegetation Index (EVI) are designed to provide consistent, spatial, and temporal comparisons of global vegetation conditions that can be used to monitor photosynthetic activity (Huete et al., 2002; Justice et al., 2002; Tucker, 1979). NDVI is defined as

$$\mathrm{NDVI} = \frac{\rho_{\mathrm{NIR}} - \rho_{\mathrm{red}}}{\rho_{\mathrm{NIR}} + \rho_{\mathrm{red}}} \tag{6}$$

where ρ_{NIR} (841–876 nm) and ρ_{red} (620–670 nm) are the surface reflectance factors for the respective MODIS near-infrared and red bands, respectively. The primary disadvantage of NDVI is the inherent non-linearity of ratio-based indices and the influence of additive noise effects, such as atmospheric path radiances. The NDVI also exhibits scaling problems and asymptotic (saturated) signals during high biomass conditions. It is very sensitive to

Table 1
The Biome Properties Look-Up Table (BPLUT) for MODIS ET

Parameter	ENF	EBF	DNF	DBF	MF	WL
*T*min_open (°C)	8.31	9.09	10.44	9.94	9.50	11.39
*T*min_close (°C)	−8.00	−8.00	−8.00	−6.00	−7.00	−8.00
VPD_close (Pa)	2500	3900	3500	2800	2700	3300
VPD_open (Pa)	650	930	650	650	650	650

Parameter	Wgrass	Cshrub	Oshrub	Grass	Crop
*T*min_open (°C)	11.39	8.61	8.80	12.02	12.02
*T*min_close (°C)	−8.00	−8.00	−8.00	−8.00	−8.00
VPD_close (Pa)	3600	3300	3700	3900	3800
VPD_open (Pa)	650	650	650	650	650

ENF: evergreen needleleaf forest; EBF: evergreen broadleaf forest; DNF: deciduous needleleaf forest; DBF: deciduous broadleaf forest; MF: mixed forest; WL: woody savannas; Wgrass: savannas; Cshrub: closed shrubland; Oshrub: open shrubland; Grass: grassland, urban and built-up, barren or sparsely vegetated; Crop: cropland.

canopy background variations, with NDVI degradation particularly strong at higher canopy background brightness (Huete et al., 2002). The enhanced vegetation index (EVI) was developed to optimize the vegetation signal with improved sensitivity in high biomass regions and improved vegetation monitoring through a decoupling of the canopy background signal and a reduction in atmosphere influences, using the equation:

$$\mathrm{EVI} = G \times \frac{\rho_{\mathrm{NIR}} - \rho_{\mathrm{red}}}{\rho_{\mathrm{NIR}} + C_1 \times \rho_{\mathrm{red}} - C_2 \times \rho_{\mathrm{blue}} + L} \tag{7}$$

where ρ is the surface reflectance in each respective band (ρ_{blue}: 459–479 nm), L is the canopy background adjustment that addresses non-linear, differential NIR and red radiant transfer through a canopy, C_1/C_2 are the coefficients of the aerosol resistance term, which use the blue band to correct for aerosol influences in the red band, and G (gain factor)=2.5. More details can be found in papers by Huete et al. (2002, 2006).

F_{C} is defined as the fraction of ground surface covered by the maximum extent of the vegetation canopy (varies between 0 and 1). Cleugh et al. (2007) calculated F_{C} using NDVI (Eq. (3)). In our Revised RS-PM algorithm, we have replaced NDVI with EVI, calculating vegetation cover fraction as:

$$F_{\mathrm{C}} = \frac{\mathrm{EVI} - \mathrm{EVI}_{\mathrm{min}}}{\mathrm{EVI}_{\mathrm{max}} - \mathrm{EVI}_{\mathrm{min}}} \tag{8}$$

where $\mathrm{EVI}_{\mathrm{min}}$ and $\mathrm{EVI}_{\mathrm{max}}$ are the signals from bare soil (LAI→0) and dense green vegetation (LAI→∞) (Gutman & Ignatov, 1998), which are set as seasonally- and geographically invariant constants 0.05 and 0.95, respectively. When Fc is bigger than 1, Fc is 1, and when Fc is less than 0, Fc is 0. We have done several sensitivity experiments, setting ($\mathrm{EVI}_{\mathrm{min}}$, $\mathrm{EVI}_{\mathrm{max}}$) as (0.01, 0.99), (0.05, 0.92), (0.11, 0.92) and (−0.5, 0.99), respectively. There is not much difference between the RMSE (less than 1.00 W/m^2), bias (about 3.00 W/m^2) and correlation coefficient (less than 0.01) from different sensitivity experiments.

Net radiation is linearly partitioned between the canopy and the soil surface using this vegetation cover fraction (F_{C}) such that:

$$A_{\mathrm{C}} = F_{\mathrm{C}} \times A$$

$$A_{\mathrm{SOIL}} = (1 - F_{\mathrm{C}}) \times A \tag{9}$$

where A_{C} and A_{SOIL} are the total net incoming radiation (A) partitioned to the canopy and soil, respectively.

2.3. Soil evaporation

To account for areas with sparse canopy cover, we have added a soil evaporation component to our Revised RS-PM algorithm. To calculate soil evaporation, the potential evaporation ($\lambda E_{\mathrm{SOIL\_POT}}$) is first calculated using the Penman–Monteith method (Eq. (1)). The total aerodynamic resistance to vapor transport (r_{tot}) is the sum of surface resistance (r_{s}) and the aerodynamic resistance for vapor transport (r_{v}) such that $r_{\mathrm{tot}}=r_{\mathrm{v}}+r_{\mathrm{s}}$ (Van de Griend, 1994). A constant r_{totc} (107 s m^{-1}) for r_{tot} is assumed globally based on observations of the ground surface in tiger-bush in southwest Niger (Wallace & Holwill, 1997), but it is corrected (rcorr) for atmospheric temperature (T) and pressure (P) (Jones, 1992) with standard conditions assumed to be T=20 °C and P=101,300 Pa.

$$\mathrm{rcorr} = \frac{1.0}{\left(\frac{273.15+T}{293.15}\right)^{1.75} \times \frac{101300}{P}}$$

$$r_{\mathrm{tot}} = r_{\mathrm{totc}} \times \mathrm{rcorr}$$

$$r_{\mathrm{totc}} = 107.0 \tag{10}$$

We assume that r_{v} (s/m) is equal to the aerodynamic resistance (r_{a}: s/m) from Eq. (1) since the values of r_{v} and r_{a} are usually very close (Van de Griend, 1994). The aerodynamic resistance (r_{a}) is parallel to both the resistance to convective heat transfer (r_{c}: s/m) and the resistance to radiative heat transfer (r_{r}: s/m) (Choudhury & DiGirolamo, 1998), such that

$$r_{\mathrm{r}} = \frac{\rho \times C_{\mathrm{p}}}{4.0 \times \sigma \times T^3}$$

$$r_{\mathrm{a}} = \frac{r_{\mathrm{c}} \times r_{\mathrm{r}}}{r_{\mathrm{c}} + r_{\mathrm{r}}} \tag{11}$$

The r_{c} is assumed to be equal to boundary layer resistance, which is calculated in the same way as total aerodynamic resistance (r_{tot}) from Eq. (10) (Thornton, 1998). Finally, the actual soil evaporation ($\lambda E_{\mathrm{SOIL}}$) is calculated in Eq. (12) using potential soil evaporation ($\lambda E_{\mathrm{SOIL\_POT}}$) and the complementary relationship hypothesis (Bouchet, 1963; Fisher et al., in press), which defines land-atmosphere interactions from vapor pressure deficit and relative humidity (RH, %).

$$\lambda E_{\mathrm{SOIL\_POT}} = \frac{sA_{\mathrm{SOIL}} + \rho C_{\mathrm{p}}(e_{\mathrm{sat}} - e)/r_{\mathrm{a}}}{s + \gamma \times \frac{r_{\mathrm{tot}}}{r_{\mathrm{a}}}}$$

$$\lambda E_{\mathrm{SOIL}} = \lambda E_{\mathrm{SOIL\_POT}} \times \left(\frac{RH}{100}\right)^{(esat-e)/100} \tag{12}$$

To examine the sensitivity of $\lambda E_{\mathrm{SOIL}}$ to r_{tot} in Eq. (10), we used different values for r_{totc} in the algorithm. The observed LE average over the 19 flux towers is 66.9 W/m^2, while the average LE estimate is 61.0 W/m^2 driven by tower meteorological data and 65.6 W/m^2 driven by GMAO data. When r_{totc} is 10 s m^{-1}, much lower than 107 s m^{-1}, soil evaporation is much higher, and hence LE is much higher, with the average tower-driven LE of 86.0 W/m^2 and GMAO-driven LE of 98.7 W/m^2. However, when r_{totc} ranges between 50 s m^{-1} and 1000 s m^{-1}, there is little difference in the soil evaporation results, and there is, therefore, little change in LE (tower-driven LE average of 54.4–64.6 W/m^2 and GMAO-driven LE average of 58.9–70.0 W/m^2). The value of 50 s m^{-1} was chosen as the lower bound because it is very close to the mean boundary layer resistance for vegetation under semiarid conditions, and there is little variation around this mean (Van de Griend, 1994). Finally, the latent heat flux for the ecosystem is calculated as the sum of the transpiration (Eq. (1)) and the soil evaporation (Eq. (12)).

3. Eddy covariance flux towers

To validate our Revised RS-PM algorithm, we used the observed latent heat flux for a number of field-based eddy covariance flux towers. The AmeriFlux network (http://public.ornl.gov/ameriflux/) was established in 1996 as a network of field sites that provide continuous observations of ecosystem level exchange of CO_2, water, and energy. AmeriFlux, part of the global Fluxnet network (Baldocchi et al., 2001), is currently comprised of 106 sites in North America, Central America, and South America. We verified the ET algorithm at 19 AmeriFlux eddy covariance tower sites (Table 2, Fig. 2) during 2001. These flux towers (Fig. 2, Table 2) cover six typical land cover types and a wide range of climates.

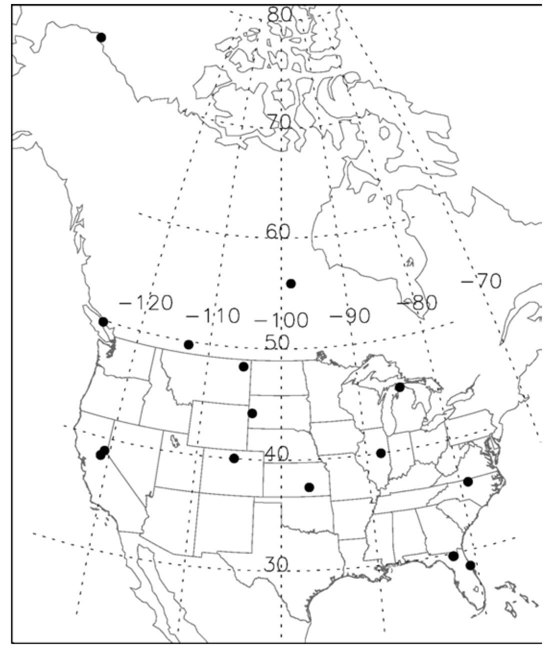

Fig. 2. Distribution of the 19 AmeriFlux eddy flux towers used for verification of the ET algorithm.

4. Data and methods

4.1. Eddy covariance flux tower sites

For each tower, we obtained the ET estimates using both the RS-PM algorithm and our Revised RS-PM algorithm, comparing the estimated ET with observations at the flux tower sites. Since the observed water vapor fluxes are the sum of the plant transpiration and soil evaporation, and it is not possible to separate the two fluxes using standard flux tower data, we compare only the total evapotranspiration estimates with the observed total ET.

4.1.1. Input datasets

For each tower and each algorithm, we estimated ET using two different sets of meteorological data: (1) integrated meteorological data derived from the half-hour observations at flux tower sites and (2) the Global Modeling and Assimilation Office (GMAO; Global Modeling and Assimilation Office, 2004) meteorological data at 1.00°×1.25° resolution. The GMAO dataset is also used in the calculation of MODIS GPP and NPP (Running et al., 2004). Remote sensing inputs include Collection 4 MODIS land cover (MOD12Q1; Friedl et al., 2002), MOD13A2 NDVI/EVI (Huete et al., 2002, 2006), MOD15A2 LAI (Myneni et al., 2002), and the 0.05° albedo from MOD43C1 (http://www-modis.bu.edu/brdf/userguide/cmgalbedo.html; Jin et al., 2003a,b; Lucht et al., 2000; Salomon et al., 2006; Schaaf et al., 2002). For each tower, we calculated the ET for the vegetated 3×3 1-km^2 MODIS pixels surrounding each site driven by the pre-processed GMAO and MODIS data as following, and

Table 2
The locations, abbreviations, biome types in the parentheses, latitude (Lat), longitude (Lon), elevation (Elev, unit: m), annual mean MODIS EVI (EVI), annual mean LAI (LAI) and the published papers for the 19 AmeriFlux eddy flux towers

Site	Abbrev.	Lat	Lon	Elev	EVI	LAI	Citation
Kennedy Space Flight Center scrub oak, FL	KSCOak (DBF)	28.61	−80.67	3	0.40	3.8	
Austin Cary, FL	AUS (ENF)	29.74	−82.22	50	0.41	4.4	Powell et al. (2005)
Donaldson, FL	Dnld (ENF)	29.75	−82.16	50	0.39	3.0	Clark et al. (2004)
Mize, FL	Mize (ENF)	29.76	−82.24	50	0.37	3.6	Clark et al. (2004)
Duke Forest hardwoods, NC	DukeHdwd (DBF)	35.97	−79.10	0	0.41	4.2	Stoy et al. (2006)
Duke Forest pine, NC	Duke_Pine (ENF)	35.98	−79.09	163	0.41	4.2	Stoy et al. (2006)
Walnut River, KS	Walnut (Grass)	37.52	−96.86	408	0.28	1.3	
Vaira Ranch, CA	Vaira (Grass)	38.41	−120.95	129	0.30	2.1	
Tonzi Ranch, CA	Tonz (Savanna)	38.43	−120.97	177	0.30	1.9	
Blodgett, CA	Blod (ENF)	38.90	−120.63	1315	0.37	3.6	Goldstein et al. (2000)
Bondville, IL	Bond (Crop)	40.01	−88.29	213	0.40	2.8	
Niwot Ridge Forest, CO	NwtR (ENF)	40.03	−105.55	3050	0.28	2.2	
Black Hills, SD	BlkHls (ENF)	44.16	−103.65	0	0.32	2.9	
Univ of Michigan, MI	UMBS (ENF)	45.56	−84.71	234	0.35	3.1	
Fort Peck, MT	FtPeck (Grass)	48.31	−105.10	634	0.16	0.4	
Lethbridge, Alberta	Leth (Grass)	49.71	−112.94	960	0.16	0.3	Flanagan et al., 2002; Wever et al., 2002
Campbell River, Vancouver Island, BC	CampRvr (ENF)	49.85	−125.32	300	0.40	3.9	
BOREAS NSA— Old Black Spruce, Manitoba	NOBS (ENF)	55.88	−98.48	259	0.25	2.5	Dunn et al., 2007; data version: June, 2006
Barrow, AK	BRW (OShrub)	71.32	−156.63	1	0.26	0.7	

averaged the ET across all pixels. These averages were then compared with the tower ET observations.

4.1.2. Pre-processing data

4.1.2.1. Tower observations. For site observations of ET and meteorology, we aggregated the half-hourly data provided by the tower researchers into daily data without using additional quality control. To maintain the integrity of the observations, no gap-filling was performed for these data.

4.1.2.2. Spatially interpolating GMAO data. The resolution for GMAO meteorological data is too coarse for a 1-km^2 MODIS pixel. Zhao et al. (2005) found that, in the Collection 4 MODIS GPP/NPP algorithm (MOD17), each 1-km pixel falling into the same 1.00°×1.25° GMAO grid cell inherited the same meteorological data, creating a noticeable GMAO footprint (Fig. 1a,c in Zhao et al., 2005). Such treatment may be acceptable on a global or regional scale, but it can lead to large inaccuracies at the local scale, especially for terrain with topographical variation or located in relatively abruptly climatic gradient zones. To enhance the meteorological inputs, Zhao et al. (2005) have non-linearly interpolated the coarse resolution GMAO data to the 1-km^2 MODIS pixel level based on the four GMAO cells surrounding a given pixel. Theoretically, this GMAO spatial interpolation improves the accuracy of meteorological data for each 1-km^2 pixel because it removes the abrupt changes from one side of a GMAO boundary to the other. In addition, for most World Meteorological Organization (WMO) stations, spatial interpolation reduced the RMSE and increased the correlation between the GMAO data and the observed WMO daily weather data for 2000–2003, suggesting that the non-linear spatial interpolation considerably improves GMAO inputs. These interpolated data were, therefore, used in our calculations of ET.

4.1.2.3. Temporally interpolating MODIS data with bad QC or missing data. The 8-day MODIS LAI (MOD15A2) (Myneni et al., 2002) and 16-day MODIS NDVI and EVI (MOD13A2) (Huete et al., 2002, 2006) contain some cloud-contaminated or missing data (Hill et al., 2006). According to the MOD15A2 quality assessment scheme provided by Myneni et al. (2002), FPAR/LAI values retrieved by the main algorithm (i.e., Radiation Transfer process, denoted as RT) are most reliable, and those retrieved by the back-up algorithm (i.e., the empirical relationship between FPAR/LAI and NDVI) are less reliable because the back-up algorithm is employed mostly when cloud cover, strong atmospheric effects, or snow/ice are detected. The LAI retrievals by the backup algorithm have low quality and should not be used for validation and other studies (Yang et al., 2006). We temporally filled the missing or unreliable LAI, NDVI, and EVI at each 1-km MODIS pixel based on their corresponding quality assessment data fields as proposed by Zhao et al. (2005). The process entails two steps (see Fig. 5 in Zhao et al., 2005). If the first (or last) 8-day LAI (16-day NDVI, EVI) is unreliable or missing, it will be replaced by the closest reliable 8-day (16-day) value. This step ensures that the second step can be performed in which other unreliable LAI (NDVI, EVI) will be replaced by linear interpolation of the nearest reliable values prior to and after the missing data point.

4.1.2.4. MODIS albedo. For MODIS albedo, we used the 10th band of the White-Sky-Albedo from the 0.05° 16-day MOD43C1 BRDF products (Jin et al., 2003a,b; Lucht et al., 2000; Salomon et al., in press; Schaaf et al., 2002; http://www-modis.bu.edu/brdf/userguide/cmgalbedo.html). This MODIS albedo is used to calculate reflected solar radiation, and hence the net incoming solar radiation. The unreliable or missing albedo data are also temporally filled with the method proposed by Zhao et al. (2005).

4.2. Data at the global scale

The input data for the global ET include the 1.00°×1.25° GMAO meteorological data and the 0.05° MODIS data as outlined in Section 4.1 for 2001. We used the same method as in Section 4.1.2.2 to get the interpolated 0.05° GMAO data, and the same method as in Section 4.1.2.4 to get the MODIS albedo for each 0.05° MODIS pixel.

4.2.1. MODIS LAI from MOD15A2

We filled the unreliable 1-km^2 LAI data using the MOD15A2 quality assessment fields and the method proposed by Zhao et al. (2005), aggregated these enhanced 1-km^2 LAI into 5-km data, and further reprojected the 5×5-km Sinusoidal data to 0.05° LAI in geographic projection. South America is the area where the

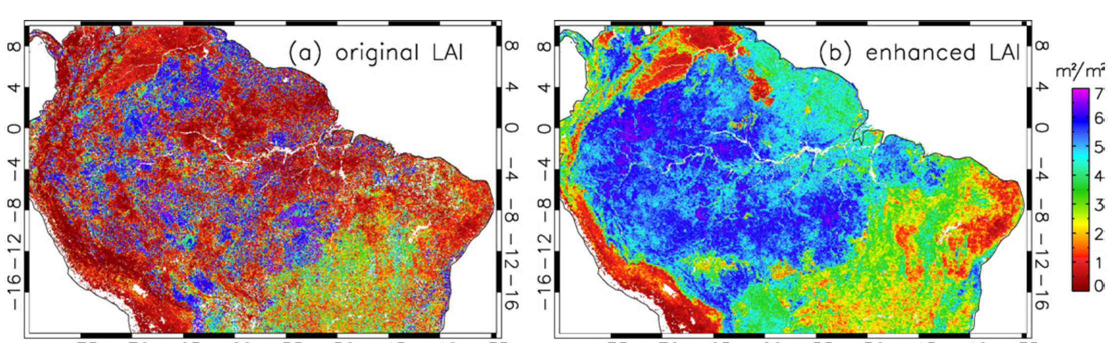

Fig. 3. The 8-day composite leaf area index (LAI) in Amazon region for the 8-day period 081 (March 21–28) in 2001 for (a) the original with no temporal interpolation of the LAI and (b) the temporally interpolated LAI.

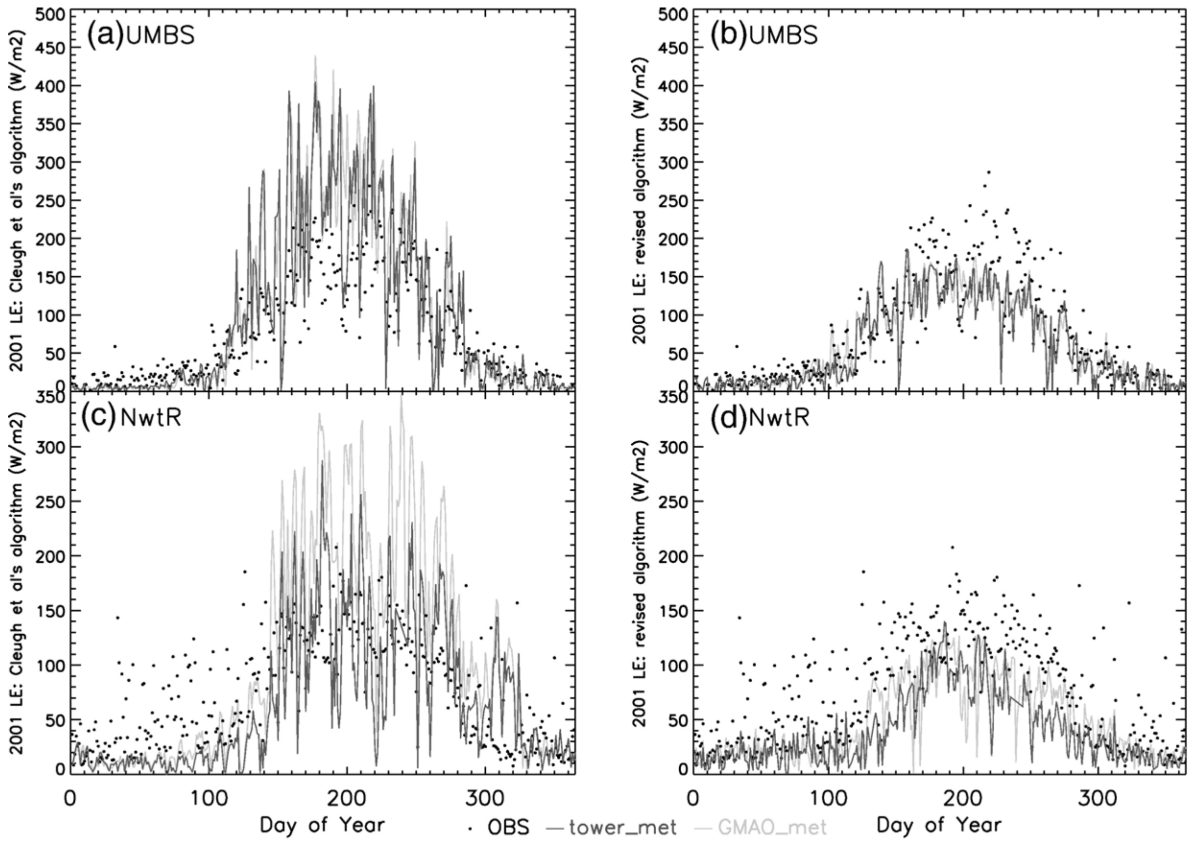

Fig. 4. The ET observations (black dots, OBS), the ET estimates driven by flux tower observed meteorological data (black lines, tower_met) and GMAO meteorological data (grey lines, GMAO_met) in 2001 from the RS-PM algorithm (a, c) and our Revised RS-PM algorithm (b, d) at two tower sites UMBS (a,b) and NwtR (c,d).

cloud contamination is the most serious and the LAI seasonality is very small. To explore how the QC-controlled interpolations alter and enhance the input MODIS data quality, we compare the 8-day composited LAI in the Amazon for the original data integrated from MOD15A2 without the temporal interpolation and the enhanced LAI values with the interpolation for the period of

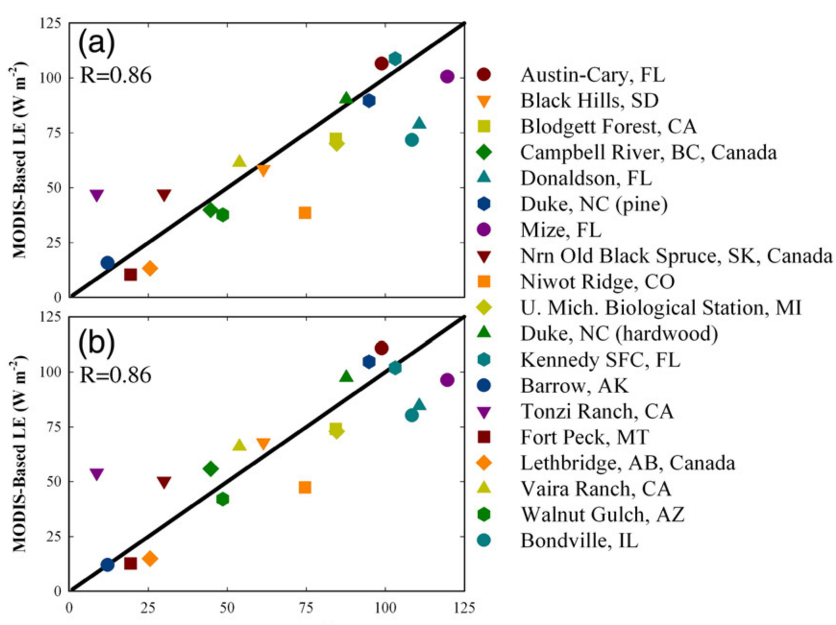

Fig. 5. Comparison of annual latent heat flux (LE) observations from the flux tower sites and the ET estimates averaged over the MODIS 3 × 3 km cutout. These data were created using (a) tower-specific meteorology and (b) the global GMAO meteorology.

March 21–28, 2001 during the wet season with the worst cloud contamination (Fig. 3). The original LAI values are too small (<2.0 m^2/m^2) for a large area surrounding the Amazon River, the result of severe cloud contamination. The MODIS land cover indicates most forests in the northern South America in Fig. 3 are evergreen broadleaf forests (EBF). Field LAI observations revealed a mean LAI of 4.8 ± 1.7 for 61 observations in tropical EBF (Asner et al., 2003; Malhi et al., 2004, 2006). There are a few pixels for which the enhanced LAI values are smaller than the original data because of the bad QCs. Overall, however, after temporal filling, LAI values in Amazon are much higher and the spatial pattern is more realistic.

4.2.2. MODIS EVI calculated from MOD43C3

Since Collection 4 MODIS data don't have a 0.05° global EVI product, we calculated the 0.05° global EVI (Eq. (7)) (Huete et al., 2002, 2006) using the 0.05° MODIS 43C3 BRDF (Bidirectional Reflectance Distribution Function) quality-controlled surface reflectance. We then filled EVI gaps due to unreliable or missing BRDF reflectance with the method proposed by Zhao et al. (2005).

5. Results and discussion

5.1. Verification at the eddy flux tower sites

The ET average over the 3×3 1-km MODIS pixels surrounding each site was compared with the tower ET observations.

Two tower sites with more than 300 days of available ET and meteorological observations in 2001 were used to compare seasonal results between the RS-PM algorithm and our Revised RS-PM algorithm. The UMBS tower (University of Michigan Biological Station) is located within a mixed deciduous–conifer forest (45.5597 °N,− 84.7138°). The glacial moraine forest at Niwot Ridge (NwtR), CO, (40.0329 °N,− 105.5464°) is a subalpine coniferous forest site. Fig. 4 (a, b) demonstrates that our

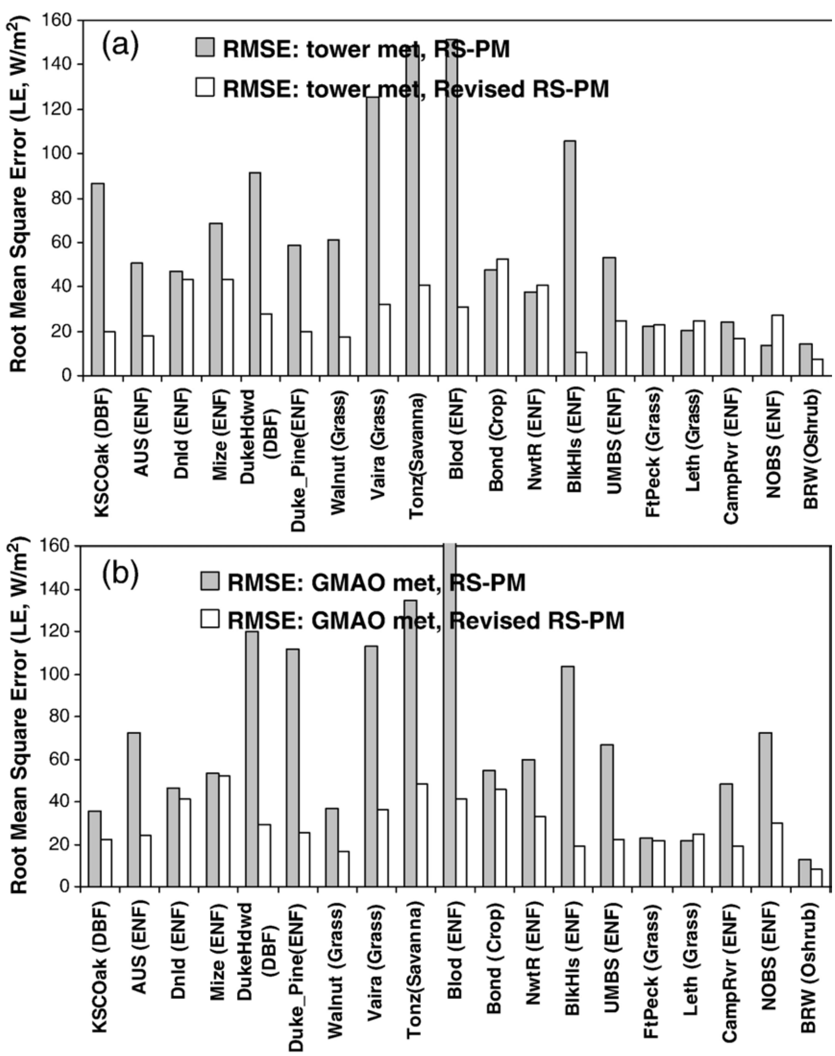

Fig. 6. Root mean square error (RMSE) between observed and calculated 8-day latent heat flux using the RS-PM and Revised RS-PM algorithms driven by (a) flux tower meteorological data (tower met) and (b) GMAO meteorological data (GMAO met). Grey columns are the RMSE between the 8-day LE observations and the LE estimates driven by Cleugh's RS-PM algorithm; white columns are those driven by our Revised RS-PM algorithm. ENF: evergreen needle-leaf forest; DBF: deciduous broadleaf forest; Oshrub: open shrub.

Table 3
The tower abbreviations, 8-day RMSE, biases (BIAS) and correlation coefficient (R) of latent heat flux for the 19 AmeriFlux eddy flux towers as in Table 2

Site	RMSE1	RMSE2	RMSE3	RMSE4
KSCOak (DBF)	86.65	35.51	19.85	22.47
AUS (ENF)	50.66	72.20	17.93	24.38
Dnld (ENF)	47.06	46.26	43.48	41.40
Mize (ENF)	68.51	53.19	43.04	52.29
DukeHdwd (DBF)	91.63	120.23	27.71	29.22
Duke_Pine (ENF)	58.86	111.67	19.79	25.22
Walnut (Grass)	61.10	36.67	17.12	16.34
Vaira (Grass)	125.60	113.10	32.06	36.26
Tonz (Savanna)	148.31	134.29	40.77	48.04
Blod (ENF)	151.16	181.59	30.63	41.48
Bond (Crop)	47.58	54.56	52.81	45.84
NwtR (ENF)	37.41	59.68	40.55	33.21
BlkHls (ENF)	105.48	103.69	10.46	19.04
UMBS (ENF)	53.14	66.96	24.52	22.37
FtPeck (Grass)	22.35	22.67	22.90	21.39
Leth (Grass)	20.36	21.60	24.75	24.74
CampRvr (ENF)	24.17	48.37	16.40	19.30
NOBS (ENF)	13.72	72.09	27.38	29.71
BRW (OShrub)	14.05	12.64	7.23	8.09
Average	64.62	71.95	27.34	29.52

Site	BIAS1	BIAS2	BIAS3	BIAS4
KSCOak (DBF)	74.43	26.35	5.73	−1.20
AUS (ENF)	43.85	63.67	7.75	11.98
Dnld (ENF)	17.13	25.92	−31.76	−26.10
Mize (ENF)	44.90	21.59	−18.99	−23.27
DukeHdwd (DBF)	80.27	97.47	2.76	9.87
Duke_Pine (ENF)	44.89	87.37	−5.13	9.87
Walnut (Grass)	37.60	16.26	−10.85	−6.45
Vaira (Grass)	90.16	84.16	7.78	12.25
Tonz (Savanna)	130.42	119.18	38.48	45.27
Blod (ENF)	121.38	154.31	−11.95	−10.18
Bond (Crop)	1.77	16.12	−36.75	−28.15
NwtR (ENF)	−12.51	20.73	−35.90	−27.18
BlkHls (ENF)	90.37	94.51	−2.85	6.53
UMBS (ENF)	30.13	35.79	−14.51	−11.65
FtPeck (Grass)	−8.82	−9.46	−8.90	−6.59
Leth (Grass)	−5.53	−9.00	−12.15	−10.57
CampRvr (ENF)	−6.45	31.31	−4.89	11.12
NOBS (ENF)	−5.83	47.60	17.31	20.29
BRW (OShrub)	−10.01	−8.69	3.68	−0.01
Average	39.90	48.17	−5.85	−1.27

Site	R1	R2	R3	R4
KSCOak (DBF)	0.89	0.89	0.84	0.80
AUS (ENF)	0.56	0.49	0.81	0.67
Dnld (ENF)	0.48	0.48	0.60	0.51
Mize (ENF)	0.68	0.62	0.81	0.72
DukeHdwd (DBF)	0.92	0.90	0.92	0.91
Duke_Pine (ENF)	0.90	0.88	0.90	0.87
Walnut (Grass)	0.91	0.88	0.90	0.87
Vaira (Grass)	0.47	0.49	0.70	0.62
Tonz (Savanna)	0.15	0.27	−0.13	−0.04
Blod (ENF)	0.80	0.87	0.86	0.67
Bond (Crop)	0.86	0.88	0.81	0.82
NwtR (ENF)	0.76	0.86	0.89	0.88
BlkHls (ENF)	0.63	0.77	0.96	0.86
UMBS (ENF)	0.96	0.95	0.95	0.96
FtPeck (Grass)	0.41	0.42	0.34	0.42
Leth (Grass)	0.67	0.66	0.66	0.57
CampRvr (ENF)	0.85	0.85	0.91	0.91
NOBS (ENF)	0.85	0.85	0.89	0.89
BRW (OShrub)	0.60	0.66	0.84	0.70
Average	0.70	0.72	0.76	0.72

1: Tower-driven results from RS-PM; 2: GMAO-driven results from RS-PM; 3: tower-driven results from Revised RS-PM; 4: GMAO-driven results from Revised RS-PM.

Revised RS-PM algorithm performs better than the RS-PM algorithm at UMBS in 2001. Our Revised RS-PM algorithm reduced the ET from nearly twice the magnitude of the observed ET data to values similar to the observations during May–September, while reducing the RMSE of the 8-day latent heat flux from 53.1 W/m^2 (62.8% of the observed annual mean) to 24.5 W/m^2 (29.0%) when the algorithm is driven by tower meteorological data, and from 67.0 W/m^2 (79.1%) to 22.4 W/m^2 (26.4%) with the GMAO meteorological data. However, Fig. 4 (c, d) shows that Revised RS-PM algorithm generally performs worse than the original ET algorithm at NwtR when driven by tower meteorological data in 2001. The ET estimates from our Revised RS-PM algorithm are much lower in spring and summer than the observations, but are much closer to the observations than those from RS-PM algorithm in autumn and winter. The RMSE of the 8-day latent heat flux driven by tower meteorological data increased from 37.4 W/m^2 (50.2% of the observed annual mean) with the RS-PM algorithm to 40.6 W/m^2 (54.4%) using Revised RS-PM algorithm. The NwtR site is located in the Roosevelt National Forest in the Rocky Mountains, sits on a glacial moraine and was established following clear-cut logging. Subalpine forest extends 2 km west of the tower. Due to the complex terrain and resulting heterogeneity of the landscape surrounding NwtR, it is possible that biases in scaling LE estimates from the flux tower to the larger 3×3 1-km^2 area would be greater than at more homogeneous sites, decreasing the inaccuracies when using larger-scale models.

Fig. 5 shows the comparison between annual latent heat flux (LE) observations measured at the nineteen flux tower sites and those estimated with our Revised RS-PM algorithm averaged over a MODIS 3×3 1-km^2 cutout. These two sets of estimated data were driven by tower-specific meteorology (Fig. 5a) and the global GMAO meteorology (Fig. 5b). The correlation coefficients between the LE observations and tower-driven algorithm estimates are $R=0.86$ ($p<0.00001$) using our Revised RS-PM algorithm and $R=0.68$ ($p=0.0014$) using RS-PM. Comparison of tower data with results driven by the GMAO meteorology resulted in correlations of $R=0.86$ ($p<0.00001$) with our Revised RS-PM algorithm and $R=0.67$ ($p=0.0017$) with RS-PM. The relative error between the 8-day averaged LE estimates driven by GMAO and tower meteorology is 14.3%, indicating that meteorology plays an important role in the accuracy of our Revised RS-PM algorithm.

Our Revised RS-PM algorithm improves the ET estimates at most of the 19 flux tower sites in 2001 compared with these estimated using the RS-PM algorithm (Fig. 6; Table 3). When driven by tower meteorological data, our Revised RS-PM

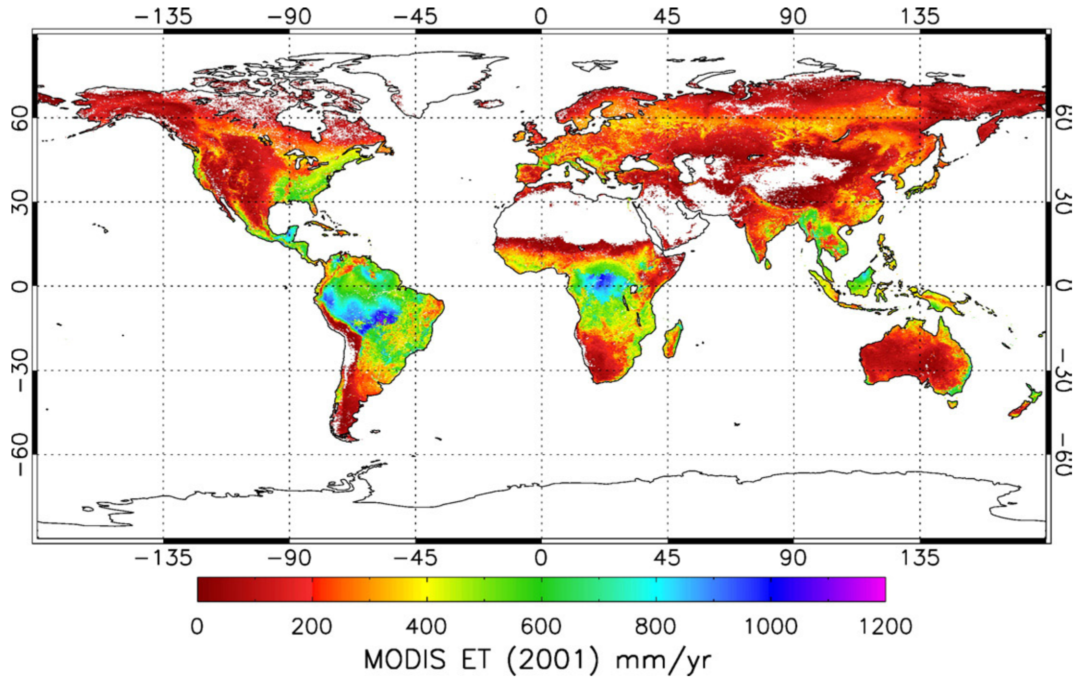

Fig. 7. Global ET driven by interpolated GMAO meteorological data and 0.05° MODIS data in 2001 with the maximum ET of 1197 mm/yr and an average ET of 286 ± 237 mm/yr for vegetated land areas. Vegetated regions are shown in color, while regions in white are barren or sparsely vegetated areas and non-vegetated areas, including water bodies, snow and ice, and urban areas.

algorithm reduced RMSE at 14 of the 19 flux tower sites, while reducing the RMSE at 18 of the 19 flux tower sites when driven by the GMAO data. The average RMSE of the 8-day latent heat fluxes over the 19 flux towers (Fig. 6; Table 3) decreased from 64.6 W/m^2 using the RS-PM algorithm to 27.3 W/m^2 with our Revised RS-PM algorithm (tower-based meteorology) and from 71.9 W/m^2 to 29.5 W/m^2 (GMAO meteorology). The correlation coefficients between the ET estimates and observations for the 8-day results are very similar from both algorithms, averaging 0.72 with GMAO meteorological data and 0.76 with tower meteorological data (Table 3). The existing biases between the ET estimates and the ET observations may be influenced by:

1) *Algorithm input data.* Heinsch et al. (2006) compared tower meteorological data with GMAO data, and the 1-km MODIS LAI (MOD15) and MODIS land cover (MOD12) with ground-based measurements, finding existing biases in both the GMAO data and the MODIS data when compared to observations. While approximately 62% of MODIS LAI estimates were within the estimates based on field optical measurements, remaining values overestimated site values (Heinsch et al., 2006). Comparison of LAI at the patch level can significantly improve the results, but MODIS LAI still tends to be higher (Wang et al., 2004). Overestimates of LAI may result in overestimates of ET even if other input data such as the meteorological data and MODIS EVI data are relatively accurate. Although the temporal filling of unreliable MODIS data, including LAI, EVI and albedo, greatly improves the accuracy of inputs, the filled values are artificial and contain uncertainties. The MODIS LAI data are generated using the Collection 3 Land Cover data (Myneni et al., 2002), while we use the Collection 4 Land Cover product in our ET calculations. While differences between the two Land Cover data products are small (unpublished data), this could lead to inaccuracies in estimating ET. The inaccuracy in MODIS EVI will lead to miscalculation of Fc, and hence ET. An extreme experiment conducted by setting Fc as 1.0 for all 19 towers shows that tower-driven RMSE increases from 27.3 W/m^2 to 40.1 W/m^2, from 29.5 W/m^2 to 49.6 W/m^2 driven by GMAO data. The average LE bias of the tower-driven LE estimates to the LE observations changed from −5.8 W/m^2 to 19.2 W/m^2 and from −1.3 W/m^2 to 31.2 W/m^2 driven by GMAO data. Finally, MOD12Q1 accuracies are in the range of 70–80%, with most mistakes between similar classes (Strahler et al., 2002). Misclassification of the land cover will result in using the wrong parameters for VPD and minimum air temperature for stomatal conductance constraints, resulting in less accurate ET estimates. When no water or air temperature stress was put on the stomatal conductance, the tower-driven RMSE increased from 27.3 W/m^2 (with stress) to 43.2 W/m^2, from 29.5 W/m^2 (with stress) to 46.3 W/m^2 driven by GMAO data. The average LE bias of the tower-driven LE estimates to the LE observations changed from −5.8 W/m^2 (with stress) to 19.9 W/m^2 and from −1.3 W/m^2 (with stress) to 23.3 W/m^2 driven by GMAO data. The correlation coefficients decreased from 0.76 (with stress) to 0.67 with the use of tower meteorological data. Water stress and air temperature stress can affect the ET estimates a lot. All of these uncertainties from inputs can introduce biases in ET estimates that are difficult to detect.
2) *Missing observation data.* The tower latent heat flux and meteorological data is typically reported at a half-hourly

interval. For seven of the 19 Ameriflux towers we used, there were fewer than 200 available days of both LE and meteorological data. For these available daily observations, there were, on average, fewer than 15 measurements per day. Using so few observation samples to obtain estimates of daily meteorology or a daily average of ET can lead errors in the analysis (Desai et al., 2005). However, most gap-filling methods have been tested on net ecosystem exchange of CO_2 and not ET, limiting our ability to obtain reliable gap-filled estimates of daily ET.

3) *Scaling from tower to landscape*. The size of the flux tower footprint is largely influenced by tower height and local environment conditions (Cohen et al., 2003; Turner et al., 2003a,b). The comparison of observed ET with the estimated from the 3×3 1-km^2 MODIS across all 19 sites may introduce uncertainties due to the differences in tower footprints for different towers and under varying environmental conditions for a given tower. In heterogeneous areas, the differing scales of the tower and MODIS ET estimates should be performed via an upscaling process, such as that used during the Bigfoot study (Cohen et al., 2003; Heinsch et al., 2006; Turner et al., 2003a,b). The expense and intensity of such studies, however, limits our ability to perform such comparisons.
4) *Algorithm limitations*. Some issues remaining in the ET algorithm might also contribute to the differences between the tower ET observations and the ET estimates by the algorithm. Biophysical parameters, such as C_L, VPD_close and VPD_open, used in the algorithm have the same values for a given biome type. However, for different species within the same biome type, the differences in these parameters can be large (Turner et al., 2003a,b). In addition, we have little knowledge regarding some parameters (e.g., boundary layer resistance for soil evaporation) and the mechanisms involved. Therefore, further study is needed to improve the ET algorithm for some ecosystems such as those in the arid areas.

5.2. Implementing ET algorithm at the global scale

These initial site-based results indicate that, although current ET estimates with our Revised RS-PM algorithm may contain biases when compared with observations, they generally agree well. The ET estimates driven by the different climate datasets are consistent at the 19 AmeriFlux sites. This suggests that we can use global reanalyzed assimilation meteorological data such as that from the GMAO together with MODIS data to estimate global ET.

Our Revised RS-PM ET algorithm was implemented globally for 2001 at a resolution of 0.05° using the preprocessed MODIS remote sensing data and the GMAO meteorological data (Fig. 7). The spatial pattern is generally reasonable, with a maximum ET of 1197 mm/yr, an average of 286 ± 237 mm/yr over vegetated land areas. As expected, tropical forests have the highest ET values, while dry areas and areas with short growing seasons have low estimates of ET. The ET for temperate and boreal forests lies between the two extremes (Fig. 7). Although there are some uncertainties, the ET magnitudes and spatial pattern of global ET generally agree with estimates provided in the literature. Evapotranspiration studies by Bruijnzeel (1990) in humid tropical forests suggest that the annual evapotranspiration ranges from 1310 to 1500 mm. Two years of combined field measurements of water vapor exchange over a Bornean tropical rainforest by Kumagai et al. (2005) show that the estimated annual evapotranspiration rates (1545 mm/yr) were at the upper limit of the range for tropical forests (Bruijnzeel, 1990; Calder et al., 1986; Leopoldo et al., 1995). Measurements of water vapor fluxes from September 1, 2003 to August 31, 2004 in a 74-year-old mixed forest in northern Ontario, Canada, reveal that the total water loss over the 12-month measurement period was 480 ± 30 mm, while total precipitation was 835 mm (Pejam et al., 2006). In data taken during 1965–1989 at 94 sites representing 11 biomes, Frank and Inouye (1994) estimate that ET ranges from 164 mm/yr in a hot desert to 1363 mm/yr in a wet tropical forest. Liski et al. (2003) reported that the ET in boreal and temperate forests across Europe (34 sites) ranged from 328 to

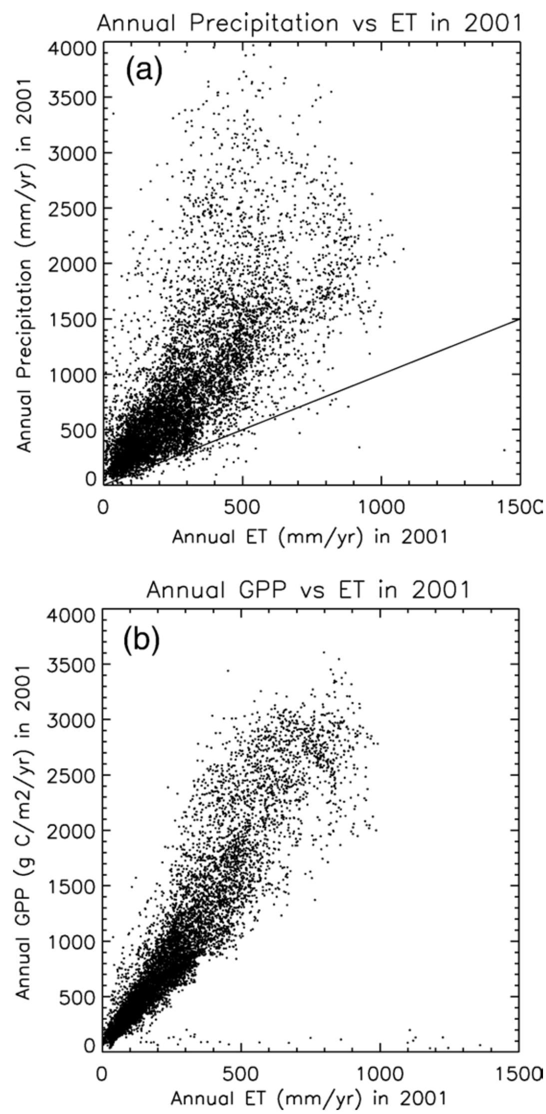

Fig. 8. (a) Annual total precipitation and (b) annual total MODIS GPP versus annual total ET (driven by GMAO meteorological data) in 2001. The solid line in (a) represents that the ratio of ET to precipitation is 1.0.

654 mm, while the average ET was 466 mm for Canada (18 sites) and 642 mm for the US and Central America (26 sites) for biomes ranging from arctic tundra to tropical rainforest.

Precipitation is not the input data to the ET algorithm, so it can be used to further verify our Revised RS-PM ET product. As expected, when the annual total Revised RS-PM ET is compared with annual total precipitation (Fig. 8a) from Chen et al. (2002) and the annual total MODIS GPP (Zhao et al., 2005) (Fig. 8b), areas with high precipitation and high GPP correspond favorably with areas with high ET. Where precipitation is high, vegetation grows well and the resulting MODIS GPP is high. Therefore, high MODIS GPP should correspond to high MODIS ET (Korner, 1994; McMurtrie et al., 1992).

To validate the global MODIS ET results, we calculated the water balance as the difference between annual precipitation from Chen et al. (2002) and annual MODIS ET (Fig. 9).

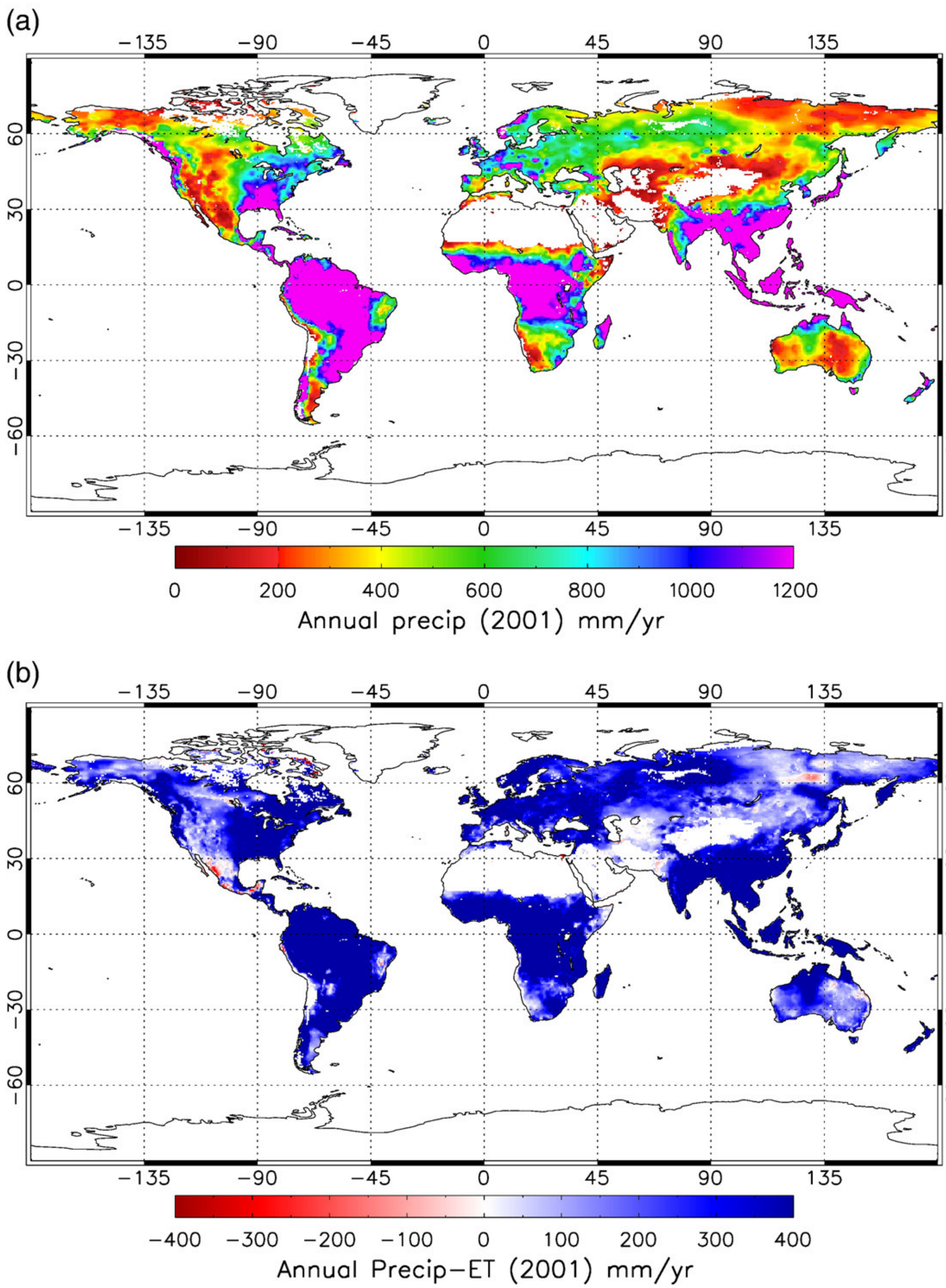

Fig. 9. (a) Global precipitation (precip) in 2001 with a maximum of 7588 mm/yr and an average of 780±686 mm/yr over land. (b) The difference between annual precipitation and annual ET (driven by GMAO meteorological data) in 2001, with a maximum of 4476 mm/yr and an average of 586±568 mm/yr. Vegetated regions are shown in color, and the regions in white are barren or sparsely vegetated areas and non-vegetated areas, including water bodies, snow and ice, and urban areas.

Theoretically, over a relatively long time period, ET should be less than precipitation (Donohue et al., 2007). Figs. 8a, 9 show that, annually, ET is less than or equal to precipitation for most vegetated pixels on the globe. However, for a number of pixels, ET is greater than precipitation, which may result from:

1) *Biases in the GMAO meteorological data.* Zhao et al. (2006) compared observed weather station data and gridded data interpolated from the observations with surface meteorological data from three well-documented global reanalyses: GMAO, European Centre for Medium-Range Weather Forecasts (ECMWF), and National Centers for Environmental Prediction/National Center for Atmospheric Research (NCEP/NCAR) reanalysis 1 to evaluate the sensitivity of the MODIS GPP/NPP to uncertainties in the meteorological inputs for both the United States and global vegetated areas. The NCEP/NCAR data tends to overestimate surface solar radiation, and underestimate both temperature and VPD. The ECMWF data have the highest accuracy but the radiation is lower in tropical regions and the accuracy of the GMAO meteorology lies between the NCEP and ECMWF (Zhao et al., 2006). Global total MODIS GPP and NPP driven by the three reanalyses datasets show notable differences (>20 Pg C/yr, average GPP: 109 Pg C/yr and average NPP: 56 Pg C/yr over 2000–2003 by GMAO) with the highest estimates from NCEP and the lowest from ECMWF. These results reveal that the biases in meteorological reanalyses can introduce substantial error. Since the incoming shortwave radiation controls the energy available for LE, and there are biases in VPD and temperature, using any of these datasets can introduce uncertainty into ET estimations.
2) *Biases in monthly precipitation.* Chen et al. (2002) obtained monthly precipitation using gauge observations from over 17,000 stations collected from the Global Historical Climatology Network (GHCN), and the Climate Anomaly Monitoring System (CAMS) datasets (Chen et al., 2002). Monthly global precipitation data over land (http://www.cpc.ncep.noaa.gov/products/global_precip/html/wpage.50yrrec.html) were reconstructed by interpolating gauge precipitation anomalies using the optimal interpolation method (Gandin, 1965). Western Europe, India, East Asia, the eastern and southwestern coastal areas of Australia, the United States, and some coastal areas of Africa and South America are covered by relatively dense gauge networks, providing more accurate data than areas in the Amazon, tropical Africa and high latitude areas where observations are sparsely distributed with notable gaps (Fig. 2 in Chen et al., 2002). In addition, there are uncertainties in gauge-measured daily precipitation. Yang et al. (2005) analyzed the precipitation at 4802 stations located north of 45 °N and concluded that the undercatch of gauge-measured precipitation is up to 22 mm/month in winter, and approximately 10 mm/month during the summer season due to wind-induced undercatch, wetting losses and trace precipitation amounts. The uncertainties in the interpolated data from the scattered observations and the interpolation procedure caused biases in the annual precipitation, which could be a primary reason why annual ET is larger than the annual precipitation for some areas, especially in the northern high latitudes (Fig. 9).
3) *Irrigation, water infiltration and subsurface runoff.* There is spatial redistribution of water from precipitation as a result of topography (e.g. Beven et al., 1995; Grayson et al., 1995; Laurenson & Mein, 1995). For example, ET is higher in arid Egypt than precipitation due to irrigation of crops using water from the Nile River, which originates in East Africa. Irrigation effects on agricultural areas of South America and the central USA might also be partially responsible for the negative differences between precipitation and evapotranspiration. In addition, Talsma and Gardner (1986) showed that some *Eucalyptus* species drew more heavily on stored soil water (ssw) during the summer of a drought year than the summers of years with average rainfall, using 200 mm more ssw than average. Donohue et al. (2007) demonstrate that ET values can exceed the energy limit for several years of unexpectedly low runoff which were preceded by moderately dry years in *Sphagnum* bogs with large water holding capacities. The observed pattern implies that the recharge/discharge of these bogs results in relatively large changes in ssw. Finally, Calder et al. (1997) reported that *Eucalyptus* plantations established on former croplands exploited substantial ssw, resulting in unusually high ET and that ssw could be up to 50% of precipitation for several years after planting. These examples demonstrate that vegetation dynamics can result in non-steady-state conditions and higher ET than precipitation, especially after vegetation change, over periods of up to several years. The longer the period needed for steady-state conditions, the more possible that ET might be higher than precipitation and the less useful the water balance of precipitation minus ET for catchment and land management applications.
4) *Issues with the MODIS ET algorithm itself.* There are still improvements that can be made to the ET algorithm. First, r_a for the plant transpiration should not be constant and r_{tot} for the soil evaporation should not be a single specified value for all biome types. In the future, we will estimate r_a and r_{tot} as functions of meteorological data, remote sensing data and different vegetation types. Second, the surface resistance (r_s) needs to be refined, and multiple-year data at additional flux towers will be used to validate and refine the algorithm.

6. Conclusions

We have revised the RS-PM ET algorithm by adding vapor pressure deficit and temperature constraints on stomatal conductance; using LAI as a scalar to estimate canopy conductance from stomatal conductance; replacing NDVI with EVI and changing the equation for the calculation of vegetation cover fraction; and adding a separate soil evaporation component to ET. The ET estimates from the RS-PM and Revised RS-PM algorithms were compared with ET observations at 19 AmeriFlux eddy flux towers driven by both site-observed daily meteorological data and GMAO reanalysis data. The verification shows that our Revised RS-PM algorithm improved ET estimates, reducing the 8-day latent heat flux biases from 64.6 W/m^2

by RS-PM algorithm to 27.3 W/m^2 driven by tower meteorological data, and from 71.9 W/m^2 to 29.5 W/m^2 driven by GMAO meteorological data. The correlation coefficients increased slightly from 0.70 to 0.76 with the use of tower meteorological data.

Daily ET estimates at the tower sites driven by GMAO data are consistent with those driven by site-based meteorological data. Due to the inclusion of several different land cover types and climates, the agreement between the ET estimates from our Revised RS-PM ET algorithm and tower ET observations implies that our Revised RS-PM ET algorithm can be implemented globally.

The global annual ET in 2001 shows reasonable spatial patterns in comparison with spatial annual MODIS GPP, annual precipitation and other studies, with areas of high ET corresponding to high GPP and high precipitation. Based on the results, our Revised RS-PM ET algorithm can be applied globally to generate near-real-time, 8-day and annual ET products, providing critical information on global terrestrial water and energy cycles and environmental changes.

Acknowledgements

This research was funded by NASA MODIS Project NNG04HZ19C. Eddy covariance flux tower sites are part of both the AmeriFlux and Fluxnet networks, and we gratefully acknowledge the efforts of researchers at these sites and thank them for making their 2001 data available. Sites are funded through grants from the U.S. Department of Energy (DOE) Office of Biological and Environmental Research (BER) unless otherwise noted. Research at the Austin, Donald, and Mize, Florida sites was led by Henry Gholz. The Black Hills, South Dakota; Bondville, Illinois; and Fort Peck, Montana, sites are supervised by Tilden Meyers. Allen Goldstein is Principal Investigator for the Blodgett Research site, California. Research at Barrow, AK, is led by Walter Oechel and was funded by the National Science Foundation (Grant No. DBI-0084157, DBI-9604793, DEB-0080754, DEB-9730004, OPP-9732105, and OPP-0119060). Andy Black provided data for the Campbell River site, and this research was funded by Forest Renewal British Columbia (1997–2000), an NSERC Strategic Grant (2000–2003), the Canadian Foundation for Innovation, and through funding for the Fluxnet Canada Research Network (NSERC, BIOCAP Canada Foundation, Canadian Foundation for Climate and Atmospheric Sciences). Dr. Black sends many thanks to his collaborators at TimberWest Forest Corp. and Weyerhaeuser Co. for allowing him to conduct this research on their land. Data from the Duke sites were gathered by Jehn-Yih Juang, Kim Novick, Mario Siqueira and Paul Stoy, and research was supported by the Office of Science (BER), U. S. Department of Energy (Grant No. DE-FG02-00ER63015), by the National Institute of Global Environmental Change (NIGEC) through the Southeast Regional Center at the University of Alabama, Tuscaloosa (DOE cooperative agreement DE-FC030-90ER61010) and by the SERC-NIGEC RCIAP Research Program. Research at the Kennedy Space Flight Center, Florida is led by Bert Drake. The research at Lethbridge, Alberta, is led by Larry Flanagan and is funded by the Natural Sciences and Engineering Council of Canada (NSERC). Funding for the Northern Old Black Spruce research site, led by Steve Wofsy and Allison Dunn, was obtained from NASA (Grant No. NAG5-11154, NAG5-7534, NAG5-2253). Research at Niwot Ridge is led by Russ Monson. Peter Curtis is Principal Investigator for research at the University of Michigan Biological Station. Dennis Baldocchi is Principal Investigator for both the Tonzi Ranch and Vaira Ranch, CA sites. Research at the Walnut River, KS, site is led by Richard Coulter. Special thanks are given to Dr. Tim McVicar and other two anonymous reviewers for providing their many good comments.

References

Asner, G. P., Scurlock, J. M. O., & Hicke, J. A. (2003). Global synthesis of leaf area index observations: Implications for ecological and remote sensing studies. *Global Ecology and Biogeography*, *12*(3), 191−205. doi:10.1046/j.1466-822X.2003.00026.x

Baldocchi, D. D., Falge, E., Gu, L. H., Olson, R., Hollinger, D., Running, S., et al. (2001). FLUXNET: A new tool to study the temporal and spatial variability of ecosystem-scale carbon dioxide, water vapour and energy flux densities. *Bulletin of the American Meteorological Society*, *82*, 2415−2434.

Bastiaanssen, W. G. M., Menenti, M., Feddes, R. A., & Holtslag, A. A. M. (1998). A remote sensing surface energy balance algorithm for land (SEBAL): 1. Formulation. *Journal of Hydrology*, *212–213*, 198−212.

Bastiaanssen, W. G. M., Menenti, M., Feddes, R. A., & Holtslag, A. A. M. (1998). The Surface Energy Balance Algorithm for Land (SEBAL): Part 2 validation. *Journal of Hydrology*, *212–213*, 213−229.

Bethenod, O., Katerji, N., Goujet, R., Bertolini, J. M., & Rana, G. (2000). Determination and validation of corn crop transpiration by sap flow measurement under field conditions. *Theoretical and Applied Climatology*, *67*, 153−160.

Beven, K., Lamb, R., Quinn, P., Romanowicz, R., & Freer, J. (1995). Topmodel. In V. P. Singh (Ed.), *Computer models of watershed hydrology* : Water Resources Publications.

Bouchet, R. J. (1963). Evapotranspiration re´elle evapotranspiration potentielle, signification climatique. *International Association of Scientific Hydrology. General Assembly of Berkeley, Transactions, vol. 2, Evaporation*. (pp. 134−142) Berkeley, Calif.

Bruijnzeel, L. A. (1990). *Hydrology of moist tropical forests and effects of conversion: A state of knowledge review.* International hydrological programme : UNESCO.

Calder, I. R., Rosier, P. T. W., Prasanna, K. T., & Parameswarappa, S. (1997). Eucalyptus water use greater than rainfall input — a possible explanation from southern India. *Hydrology and Earth System Sciences*, *1*, 249−256.

Calder, I. R., Wright, I. R., & Murdiyarso, D. (1986). A study of evaporation from tropical rain forest — West Java. *Journal of Hydrology*, *89*, 13−31.

Chen, M., Xie, P., Janowiak, J. E., & Arkin, P. A. (2002). Global Land Precipitation: A 50-yr monthly analysis based on gauge observations. *Journal of Hydrometeorology*, *3*, 249−266.

Choudhury, B. J., & DiGirolamo, N. E. (1998). A biophysical process-based estimate of global land surface evaporation using satellite and ancillary data I. Model description and comparison with observations. *Journal of Hydrology*, *205*, 164−185.

Clark, K. L., Gholz, H. L., & Castro, M. S. (2004). Carbon dynamics along a chronosequence of slash pine plantations in north Florida. *Ecological Applications*, *14*, 1154−1171.

Cleugh, H. A., Leuning, R., Mu, Q., & Running, S. W. (2007). Regional evaporation estimates from flux tower and MODIS satellite data. *Remote Sensing of Environment*, *106*, 285−304. doi:10.1016/j.rse.2006.07.007

Cohen, W. B., Maiersperger, T. K., Yang, Z., Gower, S. T., Turner, D. P., Ritts, W. D., et al. (2003). Comparisons of land cover and LAI estimates derived from ETM+ and MODIS for four sites in North America: A quality assessment of 2000/2001 provisional MODIS products. *Remote Sensing of Environment*, *88*, 233−255.

Cowan, I. R. (1977). Stomatal behaviour and environment. *Advances in Botanical Research*, *4*, 117−228.

Cowan, I. R., & Farquhar, G. D. (1977). Stomatal function in relation to leaf metabolism and environment. In D. H. Jennings (Ed.), *Society for experimental biology symposium*, *Vol. 31*. (pp. 471−505).

Dang, Q. L., Margolis, H. A., Coyea, M. R., Sy, M., & Collatz, G. J. (1997). Regulation of branch-level gas exchange of boreal trees: roles of shoot water potential and vapour pressure difference. *Tree Physiology*, *17*, 521−535.

Desai, A. R., Bolstad, P. V., Cook, B. D., Davis, K. J., & Carey, E. V. (2005). Comparing net ecosystem exchange of carbon dioxide between an old-growth and mature forest in the upper Midwest, USA. *Agricultural and Forest Meteorology*, *128*, 33−55.

Dodds, P., Meyer, W., & Barton, A. (2005). A review of methods to estimate irrigated reference crop evapotranspiration across Australia. *Technical Report 04/05, CRC for irrigation futures and CSIRO land and water, Adelaide, South Australia*.

Donohue, R. J., Roderick, M. L., & McVicar, T. R. (2007). On the importance of including vegetation dynamics in Budyko's hydrological model. *Hydrology and Earth System Sciences*, *11*, 983−995.

Dunn, A. L., Barford, C. C., Wofsy, S. C., Goulden, M. L., & Daube, B. C. (2007). A long-term record of carbon exchange in a boreal black spruce forest: means, responses to interannual variability, and decadal trends. *Global Change Biology*, *13*, 577−590. doi:10.1111/j.1365-2486.2006.01221.x

Farquhar, G. D., Buckley, T. N., & Miller, J. M. (2002). Optimal stomatal control in relation to leaf area and nitrogen content. *Silva Fennica*, *36*(3), 625−637.

Fisher, J.B., Tu, K., & Baldocchi, D.D., (in press). Global estimates of the land-atmosphere water flux based on monthly AVHRR and ISLSCP-II data, validated at FLUXNET sites. *Remote Sensing of Environment*.

Flanagan, L. B., Wever, L. A., & Carlson, P. J. (2002). Seasonal and interannual variation in carbon dioxide exchange and carbon balance in a northern temperate grassland. *Global Change Biology*, *8*, 599−615.

Frank, D. A., & Inouye, R. S. (1994). Temporal variation in actual evapotranspiration of terrestrial ecosystems: patterns and ecological implications. *Journal of Biogeography*, *21*, 401−411.

Friedl, M. A. (1996). Relationships among remotely sensed data, surface energy balance, and area-averaged fluxes over partially vegetated land surfaces. *Journal of Applied Meteorology*, *35*, 2091−2103.

Friedl, M. A., McIver, D. K., Hodges, J. C. F., Zhang, X. Y., Muchoney, D., Strahler, A. H., et al. (2002). Global land cover mapping from MODIS: Algorithms and early results. *Remote Sensing of Environment*, *83*(1–2), 287−302.

Gandin, L. S. (1965). *Objective analysis of meteorological fields.*Israel program for scientific translations. 242 pp.

Gash, J. H. C. (1987). An analytical framework for extrapolating evaporation measurements by remote sensing surface temperature. *International Journal of Remote Sensing*, *8*, 1245−1249.

Gillies, R. R., & Carlson, T. N. (1995). Thermal remote sensing of surface soil water content with partial vegetation cower for incorporation into mesoscale prediction models. *Journal of Applied Meteorology*, *34*, 745−756.

Global Modeling and Assimilation Office (2004). *File specification for GEOS-DAS gridded output version 5.3, report.* Greenbelt, Md: NASA Goddard Space Flight Cent.

Goldstein, A. H., Hultman, N. E., Fracheboud, J. M., Bauer, M. R., Panek, J. A., Xu, M., et al. (2000). Effects of climate variability on the carbon dioxide, water, and sensible heat fluxes above a ponderosa pine plantation in the Sierra Nevada (CA). *Agricultural and Forest Meteorology*, *101*(2–3), 113−129.

Granger, R. J., & Gray, D. M. (1989). Evaporation from natural nonsaturated surfaces. *Journal of Hydrology*, *111*, 21−29.

Grayson, R. B., Bloschl, G., & Moore, I. D. (1995). Distributed parameter hydrologic modeling using vector elevation data: THALES and TAPES-C. In V. P. Singh (Ed.), *Computer models of watershed hydrology* : Water Resources Publications.

Gutman, G., & Ignatov, A. (1998). Derivation of green vegetation fraction from NOAA/AVHRR for use in numerical weather prediction models. *International Journal of Remote Sensing*, *19*, 1533−1543.

Hari, P., Makela, A., Korpilahti, E., & Holmberg, M. (1986). Optimal control of gas exchange. *Tree Physiology*, *2*, 169−175.

Heinsch, F. A, Reeves, M. C., Votava, P., Kang, S., Milesi, C., Zhao, M., et al. (2003). *User's guide: GPP and NPP (MOD17A2/A3) products, NASA MODIS land algorithm* (pp. 1−57). Missoula, MT: The University of Montana.

Heinsch, F. A., Zhao, M., Running, S. W., Kimball, J. S., Nemani, R. R., Davis, K. J., et al. (2006). Evaluation of remote sensing based terrestrial productivity from MODIS using AmeriFlux tower eddy flux network observations. *IEEE Transactions on Geoscience and Remote Sensing*, *44*(7), 1908−1925.

Hill, M. J., Senarath, U., Lee, A., Zeppel, M., Nightingale, J. M., Williams, R. T., et al. (2006). Assessment of the MODIS LAI product for Australian ecosystems. *Remote Sensing of Environment.*, *101*, 495−518.

Hsiao, T., & Xu, L. (2005). *Evapotranspiration and relative contribution by the soil and the plant.* California water plan update 2005 : UC Davis.

Huete, A., Didan, K., Miura, T., Rodriguez, E. P., Gao, X., & Ferreira, L. G. (2002). Overview of the radiometric and biophysical performance of the MODIS vegetation indices. *Remote Sensing of Environment*, *83*, 195−213.

Huete, A. R., Didan, K., Shimabukuro, Y. E., Ratana, P., Saleska, S. R., Hutyra, L. R., et al. (2006). Amazon rainforests green-up with sunlight in dry season. *Geophysical Research Letters*, *33*, L06405. doi:10.1029/2005GL025583

Janowiak, J. E., Livezey, R. E., Kondragunta, A. G. C., & Huffman, G. J. (1998). Comparison of reanalysis precipitation with rain gauge and satellite observations. *Proceedings of the first WCRP international conference on reanalyses (Silver Spring, Maryland, USA, 27–31 October 1997). WCRP-104, WMO/TD-NO. 876* (pp. 207−210).

Jarvis, P. G. (1976). The interpretation of the variations in leaf water potential and stomatal conductance found in canopies in the field. *Philosophical Transactions of the Royal Society of London. Series B*, *273*, 593−610.

Jin, Y., Schaaf, C. B., Woodcock, C. E., Gao, F., Li, X., Strahler, A. H., et al. (2003). Consistency of MODIS surface BRDF/Albedo retrievals: 1. Algorithm performance. *Journal of Geophysical Research*, *108*(D5), 4158. doi:10.1029/2002JD002803

Jin, Y., Schaaf, C. B., Woodcock, C. E., Gao, F., Li, X., Strahler, A. H., et al. (2003). Consistency of MODIS surface BRDF/Albedo retrievals: 2. Validation. *Journal of Geophysical Research*, *108*(D5), 4159. doi:10.1029/2002JD002804

Jones, H. G. (1992). *Plants and microclimate: a quantitative approach to environmental plant physiology.* Cambridge, UK: Cambridge University Press.

Justice, C. O., Townshend, J. R. G., Vermote, E. F., Masuoka, E., Wolfe, R. E., Saleous, N., et al. (2002). An overview of MODIS Land data processing and product status. *Remote Sensing of Environment*, *83*, 3−15.

Kalma, J. D., & Jupp, D. L. B. (1990). Estimating evaporation from pasture using infrared thermometry: evaluation of a one-layer resistance model. *Agricultural and Forest Meteorology*, *51*, 223−246.

Kawamitsu, Y., Yoda, S., & Agata, W. (1993). Humidity pretreatment affects the responses of stomata and CO_2 assimilation to vapor pressure difference in C3 and C4 plants. *Plant Cell Physiology*, *34*(1), 113−119.

Keane, R. E., Ryan, K. C., Veblen, T. T., Allen, C. D., Logan, J., & Hawkes, B. (2002). Cascading effects of fire exclusion in Rocky Mountain ecosystems: A literature review. *USDA forest service gen. tech. report RMRS-GTR-91* 24 pp.

Korner, Ch. (1994). Leaf diffusive conductances in the major vegetation types of the globe. In E. -D. Schulze, & M. M. Caldwell (Eds.), *Ecophysiology of photosynthesis* (pp. 463−490). New York: Springer.

Kumagai, T., Saitoh, T. M., Sato, Y., Takahashi, H., Manfroi, O. J., Morooka, T., et al. (2005). Annual water balance and seasonality of evapotranspiration in a Bornean tropical rainforest. *Agricultural and Forest Meteorology*, *128*, 81−92.

Kustas, W. P, & Norman, J. M. (1996). Use of remote sensing for evapotranspiration monitoring over land surfaces. *Hydrological Sciences Journal des Sciences Hydrologiques*, *41*, 495−516.

Kustas, W. P, & Norman, J. M. (1999). Evaluation of soil and vegetation heat flux predictions using a simple two-source model with radiometric temperatures for partial canopy cover. *Agricultural and Forest Meteorology*, *94*, 13−29.

Landsberg, J. J., & Gower, S. T. (1997). *Applications of physiological ecology to forest management.* : Academic Press.

Laurenson, E. M., & Mein, R. G. (1995). RORB: hydrograph synthesis by runoff routing. In V. P. Singh (Ed.), *Computer models of watershed hydrology* : Water Resources Publications.

Leopoldo, P. R., Franken, W. K., & Villa Nova, N. A. (1995). Real evapotranspiration and transpiration through a tropical rain forest in central Amazonia as estimated by the water balance method. *Forest Ecology and Management*, *73*, 185−195.

Leuning, R. (1995). A critical appraisal of a combined stomatal-photosynthesis model for C3 plants. *Plant, Cell and Environment*, *18*, 339−355.

Liski, J., Nissinen, A., Erhard, M., & Taskinen, O. (2003). Climatic effects on litter decomposition from Arctic tundra to tropical rainforest. *Global Change Biology*, *9*(4), 575−584. doi:10.1046/j.1365-2486.2003.00605.x

Los, S. O., Collatz, G. J., Sellers, P. J., Malmstrom, C. M., Pollack, N. H., DeFries, R. S., et al. (2000). A global 9-yr biophysical land surface dataset from NOAA AVHRR data. *Journal of Hydrometeorology*, *1*(2), 183−199.

Lucht, W., Schaaf, C. B., & Strahler, A. H. (2000). An Algorithm for the retrieval of albedo from space using semiempirical BRDF models. *IEEE Transactions on Geoscience and Remote Sensing*, *38*, 977−998.

Maddock, T., III, MacNish, R., Goodrich, D., Williams, D., Shuttleworth, J., Goff, B., et al. (1998, Jan. 11–16). An overview of atmospheric and surface water coupling to regional groundwater models in semi-arid basins. *Proc. Amer. soc. of Meteorol., special symp. on hydrology, Phoenix, AZ* (pp. 38−42).

Maidment, D. R. (Ed.). (1993). *Handbook of hydrology* New York: McGraw Hill.

Malhi, Y., Baker, T. R., Phillips, O. L., Almeida, S., Alvarez, E., Arroyo, L., et al. (2004). The above-ground coarse wood productivity of 104 Neotropical plots. *Global Change Biology*, *10*(5), 563−591. doi:10.1111/j.1529-8817.2003.00778.x

Malhi, Y., Wood, D., Baker, T. R., Wright, J., Phillips, O. L., Cochrane, T., et al. (2006). The regional variation of aboveground live biomass in old-growth Amazonian forests. *Global Change Biology*, *12*(7), 1107−1138. doi:10.1111/j.1365-2486.2006.01120.x

Marsden, B. J., Lieffers, V. J., & Zwiazek, J. J. (1996). The effect of humidity on photosynthesis and water relations of white spruce seedlings during the early establishment phase. *Canadian Journal of Forest Research*, *26*, 1015−1021.

McMurtrie, R. E., Leuning, R., Thompson, W. A., & Wheeler, A. M. (1992). A model of canopy photosynthesis and water use incorporating a mechanistic formulation of leaf CO_2 exchange. *Forest Ecology and Management*, *52*, 261−278.

McVicar, T. R., & Jupp, D. L. B. (1998). The current and potential operational uses of remote sensing to aid decisions on drought exceptional circumstances in Australia: A review. *Agricultural Systems*, *57*, 399−468.

McVicar, T. R., & Jupp, D. L. B. (1999). Estimating one-time-of-day meteorological data from standard daily data as inputs to thermal remote sensing based energy balance models. *Agriculture and Forest Meteorology*, *96*, 219−238.

McVicar, T. R., & Jupp, D. L. B. (2002). Using covariates to spatially interpolate moisture availability in the Murray–Darling Basin: A novel use of remotely sensed data. *Remote Sensing of Environment*, *79*, 199−212.

Meyer, W. (1999). Standard reference evaporation calculation for inland, south eastern Australia. *Technical report 35/98* Adelaide, South Australia: CSIRO Land and Water.

Misson, L., Panek, J. A., & Goldstein, A. H. (2004). A comparison of three approaches to modeling leaf gas exchange in annually drought-stressed Ponderosa pine forests. *Tree Physiology*, *24*, 529−541.

Monteith, J. L. (1964). Evaporation and environment. The state and movement of water in living organisms. *Symposium of the society of experimental biology*, *Vol. 19*. (pp. 205−234)Cambridge: Cambridge University Press.

Morton, F. I. (1983). Operational estimates of areal evapotranspiration and their significance to the science and practice of hydrology. *Journal of Hydrology*, *66*, 1−76.

Mu, Q., Zhao, M., Heinsch, F. A., Liu, M., Tian, H., & Running, S. W. (2007). Evaluating water stress controls on primary production in biogeochemical and remote sensing based models. *Journal of Geophysical Research*, *112*, G01012. doi:10.1029/2006JG000179

Murray, F. W. (1967). On the computation of saturation vapor pressure. *Journal of Applied Meteorology*, *6*, 203−204.

Myneni, R. B., Hoffman, S., Knyazikhin, Y., Privette, J. L., Glassy, J., Tian, Y., et al. (2002). Global products of vegetation leaf area and fraction absorbed PAR from year one of MODIS data. *Remote Sensing of Environment*, *83*(1–2), 214−231.

Nemani, R. R., & Running, S. W. (1989). Estimation of regional surface resistance to evapotranspiration from NDVI and thermal infrared AVHRR data. *Journal of Applied Meteorology*, *28*, 276−284.

Nishida, K., Nemani, R., et al. (2003). Development of an evapotranspiration index from Aqua/MODIS for monitoring surface moisture status. *IEEE Transactions on Geoscience and Remote Sensing*, *41*(2).

Norman, J. M., Kustas, W. B., & Humes, K. S. (1995). Source approach for estimating soil and vegetation energy fluxes in observations of directional radiometric surface temperature. *Agricultural and Forest Meteorology*, *77*, 263−293.

Oren, R., Sperry, J. S., Katul, G. G., Pataki, D. E., Ewers, B. F., Phillips, N., et al. (1999). Survey and synthesis of intra- and interspecific variation in stomatal sensitivity to vapour pressure deficit. *Plant, Cell and Environment*, *22*, 1515−1526.

Oren, R., Sperry, J. S., Ewers, B. E., Pataki, D. E., Phillips, N., & Megonigal, J. P. (2001). Sensitivity of mean canopy stomatal conductance to vapor pressure deficit in a flooded *Taxodium distichum* L. forest: hydraulic and non-hydraulic effects. *Oecologia*, *126*, 21−29.

Pejam, M. R., Arain, M. A., & McCaughey, J. H. (2006). Energy and water vapour exchanges over a mixedwood boreal forest in Ontario, Canada. *Hydrological Processes*, *20*, 3709−3724. doi:10.1002/hyp.6384

Powell, T. L., Starr, G., Clark, K. L., Martin, T. A., & Gholz, H. L. (2005). Ecosystem and understory water and energy exchange for a mature, naturally regenerated pine flatwoods forest in north Florida. *Canadian Journal of Forest Research*, *35*, 1568−1580.

Rango, A., & Shalaby, A. I. (1998). Operational applications of remote sensing in hydrology: Success, prospects and problems. *Hydrological Sciences Journal des Sciences Hydrologiques*, *43*, 947−968.

Raupach, M. R. (2001). Combination theory and equilibrium evaporation. *Quarterly Journal of the Royal Meteorological Society*, *127*, 1149−1181.

Running, S. W., & Nemani, R. R. (1988). Relating seasonal patterns of the AVHRR Vegetation Index to simulate photosynthesis and transpiration of forests in different climates. *Remote Sensing of Environment*, *24*, 347−367.

Running, S. W., Nemani, R. R., Heinsch, F. A., Zhao, M., Reeves, M. C., & Hashimoto, H. (2004). A continuous satellite-derived measure of global terrestrial primary production. *BioScience*, *54*, 547−560.

Running, S. W, Thornton, P. E., Nemani, R. R., & Glassy, J. M. (2000). Global terrestrial gross and net primary productivity from the Earth Observing System. In O. Sala, R. Jackson, & H. Mooney (Eds.), *Methods in ecosystem science* (pp. 44−57). New York: Springer–Verlag.

Salomon, J., Schaaf, C. B., Strahler, A. H., Gao, F., & Jin, Y. (2006). Validation of the MODIS Bidirectional Reflectance Distribution Function and Albedo Retrievals using combined observations from the aqua and terra platforms. *IEEE Transactions on Geoscience and Remote Sensing*, *44*(6), 1555−1565.

Sandford, A. P., & Jarvis, P. G. (1986). Stomatal responses to humidity in selected conifers. *Tree Physiology*, *2*, 89−103.

Saugier, B., Granier, A., Pontailler, J. Y., Dufrene, E., & Baldocchi, D. D. (1997). Transpiration of a boreal pine forest measured by branch bag, sap flow and micrometeorological methods. *Tree Physiology*, *17*, 511−519.

Schaaf, C. B., Gao, F., Strahler, A. H., Lucht, W., Li, X., Tsang, T., et al. (2002). First operational BRDF, Albedo and Nadir Reflectance Products from MODIS. *Remote Sensing of Environment*, *83*, 135−148.

Schulze, E. D., Kelliher, F. M., Körner, C., Lloyd, J., & Leuning, R. (1994). Relationships among maximum stomatal conductance, ecosystem surface conductance, carbon assimilation rate, and plant nitrogen nutrition: A global ecology scaling exercise. *Annual Review of Ecology and Systematics*, *25*, 629−660.

Stoy, P. C., Katul, G. G., Siqueira, M. B. S., Juang, J., Novick, K. A., McCarthy, H. R., et al. (2006). Separating the effects of climate and vegetation on evapotranspiration along a successional chronosequence in the southeastern U.S. *Global Change Biology*, *12*, 2115−2135. doi:10.1111/j.1365-2486.2006.01244.x

Strahler, A.H., M. Friedl, X. Zhang, J. Hodges, C.S.A. Cooper, A. Baccini, (2002). The MODIS Land Cover and Land Cover Dynamics Products. *Presentation at Remote Sensing of the Earth's Environment from TERRAQ in L'Aquila, Italy.*

Su, Z. (2002). The surface energy balance system (SEBS) (for estimation of turbulent heat fluxes. *Hydrology and Earth System Sciences*, *6*, 85−99.

Talsma, T., & Gardner, E. A. (1986). Soil–water extraction by a mixed Eucalypt forest during a drought period. *Australian Journal of Soil Research*, *24*, 25−32.

Thornton, P.E. (1998) Regional ecosystem simulation: combining surface- and satellite-based observations to study linkages between terrestrial energy and mass budgets. PhD. *Dissertation, School of Forestry, The University of Montana, Missoula, MT.*, 280 pp.

Tucker, C. J. (1979). Red and photographic infrared linear combinations for monitoring vegetation. *Remote Sensing of Environment*, *8*, 127−150.

Turner, D. P., Ritts, W. D., Cohen, W. B., Gower, S. T., Zhao, M., Running, S. W., et al. (2003). Scaling gross primary production (GPP) over boreal and deciduous forest landscapes in support of MODIS GPP product validation. *Remote Sensing of Environment*, *88*, 256−270.

Turner, D. P., Urbanski, S., Bremer, D., Wofsy, S. C., Meyers, T., Gower, S. T., et al. (2003). A cross-biome comparison of daily light use efficiency for gross primary production. *Global Change Biology*, *9*, 383−395.

Van de Griend, A. A. (1994). Bare soil surface resistance to evaporation by vapor diffusion under semiarid conditions. *Water Resources Research*, *30*, 181−188.

Villalobos, F. J., & Fereres, E. (1990). Evaporation measurements beneath corn, cotton, and sunflower canopies. *Agronomy Journal*, *82*, 1153−1159.

Vörösmarty, C. J., Federer, C. A., & Schloss, A. L. (1998). Potential evaporation function compared on US watersheds: Possible implication for global-scale water balance and terrestrial ecosystem. *Journal of Hydrology*, *207*, 147−169.

Wallace, J. S., & Holwill, C. J. (1997). Soil evaporation from Tiger-Bush in South-West Niger. *Journal of Hydrology*, *188–189*, 426−442.

Wan, Z., Zhang, Y., Zhang, Q., & Li, Z. -L. (2002). Validation of the land-surface temperature products retrieved from Terra Mode rate Resolution Imaging Spectroradiometer data. *Remote Sensing of Environment*, *83*, 163−180.

Wang, Y., Woodcock, C. E., Buermann, W., Sternberg, P., Voipoi, P., Smolander, H., et al. (2004). Evaluation of the MODIS LAI algorithm at a coniferous forest site in Finland. *Remote Sensing of Environment*, *91*, 114−127.

Wever, L. A., Flanagan, L. B., & Carlson, P. J. (2002). Seasonal and interannual variation in evapotranspiration, energy balance and surface conductance in a northern temperate grassland. *Agricultural and Forest Meteorology*, *112*, 31−49.

Wilson, K. B., Hansonb, P. J., & Baldocchi, D. D. (2000). Factors controlling evaporation and energy partitioning beneath a deciduous forest over an annual cycle. *Agricultural and Forest Meteorology*, *102*, 83−103.

Xu, L., & Baldocchi, D. D. (2003). Seasonal trend of photosynthetic parameters and stomatal conductance of blue oak (*Quercus douglasii*) under prolonged summer drought and high temperature. *Tree Physiology*, *23*, 865−877.

Yang, W., Huang, D., Tan, B., Stroeve, J. C., Shabanov, N. V., Knyazikhin, Y., et al. (2006). Analysis of leaf area index and fraction of PAR absorbed by vegetation products from the terra MODIS sensor: 2000–2005. *IEEE Transactions on Geoscience and Remote Sensing*, *44*(7), 1829−1842. doi:10.1109/TGRS.2006.871214 (Part 1).

Yang, D., Kane, D., Zhang, Z., Legates, D., & Goodison, B. (2005). Bias corrections of long-term (1973–2004) daily precipitation data over the northern regions. *Geophysical Research Letters*, *32*, L19501. doi:10.1029/2005GL024057

Zhao, M., Heinsch, F. A., Nemani, R., & Running, S. W. (2005). Improvements of the MODIS terrestrial gross and net primary production global data set. *Remote Sensing of Environment*, *95*, 164−176.

Zhao, M., Running, S. W., & Nemani, R. R. (2006). Sensitivity of Moderate Resolution Imaging Spectroradiometer (MODIS) terrestrial primary production to the accuracy of meteorological reanalyses. *Journal of Geophysical Research*, *111*, G01002. doi:10.1029/2004JG000004